

Capabilities and limitations of existing hypersonic facilities

Sangdi Gu^{*}, Herbert Olivier

Shock Wave Laboratory, RWTH Aachen University, Templergraben 55, 52062, Aachen, Germany



ARTICLE INFO

Keywords:

Hypersonics
Impulse facilities
Expansion tunnels
Shock tunnels
Ground simulation
Flow characterization

ABSTRACT

This paper presents an overview and analysis of the various aspects of hypersonic ground testing. For this, first the simulation requirements according to the different flow regimes of hypersonics flight are briefly described. Based hereon the methodologies of hypersonic ground testing are reviewed and the limitations of applicability are discussed. The characteristics and capabilities of the different hypersonic wind tunnels which facilitate hypersonic ground testing are discussed. The capabilities and limitations of these facilities are quantitatively assessed in regards to the simulation of relevant flight conditions. In addition, limitations of the ground test facilities, such as test time and test model size, are assessed for reflected shock tunnels and expansion tunnels. The trend is that each type of hypersonic facility has its own unique advantages and disadvantages. Continuous running and blowdown facilities allow the longest running times, detailed measurements and best knowledge of freestream properties, but are limited to low stagnation enthalpies. On the other hand, reflected shock tunnels and especially expansion tunnels allow for high enthalpy conditions, but suffer from short test times and a limited variety of measurement techniques. So, success in experimental hypersonics would result from testing in a variety of different facilities in order to benefit from the advantages of each facility. Testing in shock tubes i.e. behind the incident shock wave is not considered in this paper since this type of experiments is mostly suitable for fundamental shock relaxation studies and not for detailed wind tunnel model testing.

1. Introduction

Research in the field of hypersonics is crucial for both national defence and space exploration purposes. Experimental hypersonics encompasses a significant portion of hypersonics research involving blunt bodies, slender bodies and propulsion systems. Experimental data is important for the validation of numerical codes, numerical simulation of the flowfield around flight vehicles and investigation of fundamental flow physics. Specific ground testing methodologies and facilities have been developed explicitly for hypersonic flows. The ground testing methodologies allow experimental data of subscale test models to be related to flight conditions. Due to driving power requirements and other constraints most of the hypersonic ground testing facilities are of intermittent or impulsive type, which therefore represents the biggest part of this paper.

The first period of hypersonic ground testing activity began in the late 1950s and continued through the 1960s, arising from the many hypersonic flight design projects and the feeling that theoretical knowledge of hypersonic flows was undeveloped [1]. During this period, numerous facilities were developed which generated hypersonic flows

by reducing the temperature of the test gas through expansion to as low as possible while adding as little energy as possible to the test gas to increase its velocity. These are called ‘cold’ facilities and they allow for the simulation of high Mach numbers but not high velocities. At the same time, ‘hot’ facilities which produced hypersonic flows by expansion of high temperature gas in a reservoir were introduced and these facilities allow for the simulation of high velocities. A second period of intense activity began in the mid-1980s and continued into the 1990s during which the National Aerospace Plane project in the USA, the ‘HOPE’ re-entry glider project from Japan and the ‘Hermes’ re-entry glider project from Europe were active. It was during this period that the free-piston driver technique was successfully applied which, along with the detonation driver technique, unlocked previously unattainable performance envelopes for ground test facilities.

In this paper, the characteristics, capabilities and limitations of different hypersonic test facilities and driver techniques are discussed. The capabilities and limitations of these facilities are quantitatively assessed in regards to the simulation of relevant flight vehicles. In addition, further limitations of the ground test facilities, such as test time and test model size, are assessed for reflected shock tunnels and

* Corresponding author.

E-mail address: gu@swl.rwth-aachen.de (S. Gu).

expansion tunnels which are currently the two most important facility types for high enthalpy hypersonics research. Additionally, the often unavoidable problem of producing thermochemically excited test flows in high enthalpy facilities with stagnated nozzle reservoir flow is reviewed.

2. Ground simulation methodology

While ground test facilities are often used to study the flow past generic models such as cylinders, spheres and wedges for fundamental investigation of specific phenomena, a significant portion of experimental work in hypersonics involves reproducing flows past actual aircrafts and space crafts for engineering purposes. However, ground test facilities generally cannot test a full scale flight vehicle over a complete range of flight conditions. Consequently, it is necessary to discuss the methodologies to simulate hypersonic flows over flight vehicles using ground test facilities.

2.1. Aerodynamic flow fields

2.1.1. Low enthalpy flows

Hornung in 1988 [2] reported a good strategy for subscale simulation of hypersonic aerodynamic flow fields. The lowest speeds at which chemical reactions become an important part of the flow field are about 2 km/s in blunt body air flows at sea level conditions. This corresponds to a stagnation temperature of about 2000 K. According to Fig. 1, at speeds below 2 km/s, the perfect gas model applies for air as the isentropic exponent, γ , is either constant or varies only with temperature due to vibrational excitation. In this case any dimensionless quantity, Q , will depend on the dimensionless parameters of the flow. If the gas used is the same between flight and experiment, the model is scaled exactly with the flight vehicle and the model and flight vehicle are orientated in the same way relative to the flow [2],

$$Q = Q\left(M_\infty, Re, \frac{T_w}{T_0}, F_q\right) \quad (1)$$

where M_∞ is the Mach number, Re is the Reynolds number, T_w/T_0 is the wall temperature to total temperature ratio and F_q is a set of dimensionless parameters defining the flow quality in the wind tunnel. This is called the Mach-Reynolds-Simulation [2].

The importance of simulating M_∞ , Re and T_w/T_0 is clear when observing, exemplarily, the rearranged flat plate laminar boundary layer thickness equation given by Ginoux [5].

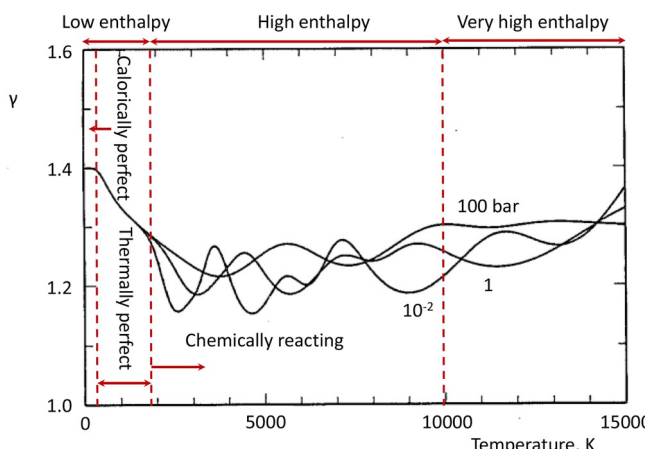


Fig. 1. Variation of the isentropic exponent, γ , of air with temperature and pressure [3].

$$\frac{\delta}{x} = \sqrt{\frac{C^*}{Re_{\infty,x}}} \left(3.07 + \frac{0.58(\gamma - 1)}{2} M_\infty^2 + \frac{1.93 T_w}{T_\infty} \right) \quad (2)$$

where δ is the boundary layer thickness, x is the distance downstream of the leading edge, $Re_{\infty,x}$ is the Reynolds number at the location x , C^* is the Chapman-Rubesin factor evaluated at the reference temperature, M_∞ is the freestream Mach number and T_∞ is the freestream temperature. From equation (2), M_∞ and the T_w/T_∞ ratio, which is matched when M_∞ and T_w/T_0 in equation (1) are matched under perfect gas conditions, are particularly important parameters for simulating the boundary layer thickness, while the Reynolds number also needs to be simulated. For typical hypersonic flight vehicles (altitude = 35 km, $M_\infty = 6$, $T_\infty = 237$ K, recovery temperature, $T_r = 1670$ K), T_w/T_∞ has a value of around 4–5. In cold hypersonic facilities where T_∞ can be around 60–80 K, using room temperature test models conveniently preserves the T_w/T_∞ ratio. However, in situations where wind tunnels are used to generate higher stagnation temperatures, e.g. in order to duplicate the total enthalpy and therewith the real flight velocity or real gas effects, which may influence viscous effects such as transition [6], heated test models must be used in order to preserve T_w/T_∞ [7]. Consider a flat plate in a typical short duration wind tunnel flow with $M_{\infty,wt} = 6$, $T_{\infty,wt} = 237$ K and $T_{w,wt} = 300$ K i.e. $(T_w/T_\infty)_{wt} = 1.3$, and a flat plate in flight with the same M_∞ and T_∞ i.e. same recovery temperature, but a wall temperature of $T_{w,fl} = 1185$ K i.e. $(T_w/T_\infty)_{fl} = 5$. Further it is assumed that the Reynolds number for flight and wind tunnel are the same which is a requirement of equation (1). Then for the considered case from equation (2), it follows:

$$\frac{\left(\frac{\delta}{x}\right)_{wt}}{\left(\frac{\delta}{x}\right)_{fl}} = 0.64 \quad (3)$$

where subscripts wt and fl denote wind tunnel and flight respectively, resulting in large differences in the boundary layer thickness at any given point behind the leading edge if the wall to freestream temperature ratio is not preserved. Hence, for these cases heated models must be used for simulating wall temperature effects in the laboratory. It has been shown that the wall temperature ratio strongly influences the size of separation bubbles [7]. It further influences the transition behaviour of boundary layers. Additionally, the heated model technique is also useful on blunt bodies in order to study ablation-radiation coupling as pioneered by Zander et al. [8].

On the other hand, the skin friction coefficient,

$$C_f = \frac{0.664}{\sqrt{Re_{\infty,x}}} \sqrt{C^*} \quad (4)$$

and the Stanton number,

$$St = \frac{0.41}{\sqrt{Re_{\infty,x}}} \sqrt{C^*} \quad (5)$$

have lower dependencies on M_∞ and T_w/T_∞ within a Mach number range that is not too large, as shown by equations (4) and (5) for a laminar boundary layer and illustrated in Fig. 2. Hence more leniency on abiding by equation (1) may be given to the simulation of the skin friction coefficient and the Stanton number which depends strongly on the geometry instead. Furthermore, included in F_q in equation (1) are parameters related to the freestream noise level, freestream turbulence level and the surface roughness. These parameters are important for studies such as boundary layer transition. Current difficulties include defining the freestream noise and turbulence levels in high enthalpy facilities and, to a lesser extent, scaling the surface roughness in subscale test models so as to prevent artificial boundary layer transition or enhanced heating rates due to surface roughness [9]. In practice, since the surface roughness needs to be scaled with the model size, a surface

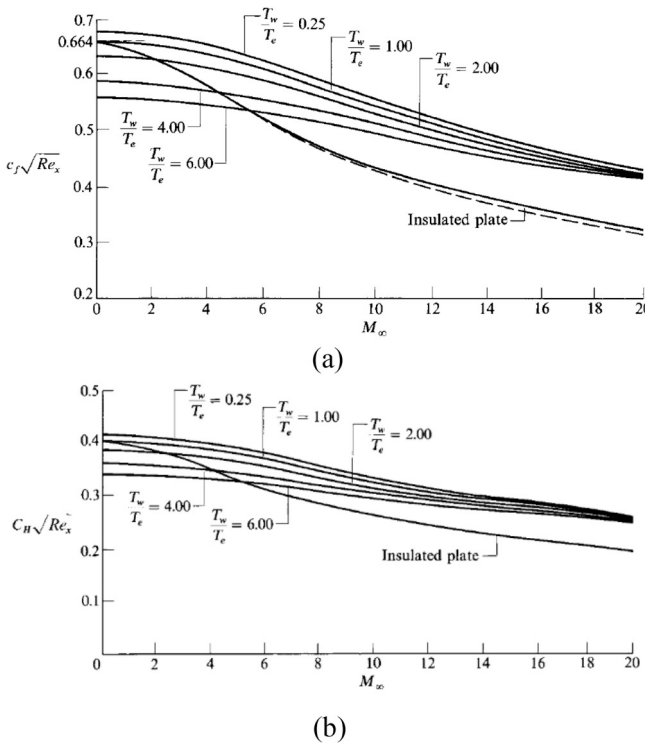


Fig. 2. Flat plate skin friction coefficient, (a), and Stanton numbers, (b), for compressible laminar boundary layers [4].

roughness of the order of 0.01 mm or even less is often required on the experimental test model, which is not always easy to obtain.

Another phenomenon of interest in hypersonic flows is the entropy layer. Correct simulation of the entropy layer is important as it can influence the heat flux distribution, skin friction, separation behaviour and boundary layer transition. For calorically perfect air at hypersonic conditions ($M_\infty > 1$), the entropy change, Δs , across a normal shock can be written as,

$$\Delta s = R * \ln(2.78 * 10^{-3} * M_\infty^5) \quad (6)$$

where R is the specific gas constant of air. The equation above shows that the entropy layer is strongly dependent on the Mach number. Hence, the duplication of the Mach number is important for the duplication of the entropy layer. The duplication of the Mach number is also important for the duplication of the laminar viscous interaction. The laminar viscous interaction parameter, $\bar{\chi}$, is given by,

$$\bar{\chi} = \frac{M_\infty^3}{\sqrt{Re_{\infty,x}}} \quad (7)$$

where C_∞ is the Chapman-Rubesin factor. The above equation shows that the Mach number has a strong influence on the viscous interaction while the Reynolds number and the wall temperature, which influences the value of C_∞ , have weaker influence on the viscous interaction.

2.1.2. High enthalpy flows

For high enthalpy flows in principle the same requirements hold as those formulated in the previous subchapter for the low enthalpy flow regime. But at speeds greater than 2 km/s or about 2000 K total temperature in blunt body air flows, additional real-gas effects become important as shown in Fig. 1 where γ varies with both temperature and pressure due to chemical reactions. A portion of hypersonic flows involves situations where dissociation reactions are dominant. In these situations, preserving the binary scaling product, $\rho_\infty L$ where ρ_∞ is the freestream density and L is the characteristic length, preserves the

normalized distribution of the chemical composition behind a shock wave. This law was first mentioned by Birkhoff in 1955 [10]. From Anderson [4], the binary scaling law can be derived as follows: for simplicity consider a two-dimensional flow where the dominant chemical reaction is the oxygen dissociation reaction, $O_2 + M \rightarrow 2O + M$ where M is the collision partner, the species continuity equation for atomic oxygen can be written as,

$$u \left(\frac{dc_O}{dx} \right) + v \left(\frac{dc_O}{dy} \right) = \frac{M_O k_f}{\rho} \left(\frac{\rho c_{O_2}}{M_{O_2}} \right) \left(\frac{\rho c_M}{M_M} \right) \quad (8)$$

where c_O and c_{O_2} is the mass fraction of O and O_2 respectively, u and v is the flow velocity in the x and y directions respectively, M_O , M_{O_2} and M_M is the molar mass of O, O_2 and M respectively, ρ is the flow density and k_f is the forward reaction rate constant which is a function of temperature as described by the Arrhenius equation. Defining the nondimensional variables $x' = x/L$, $y' = y/L$, $u' = u/U_\infty$, $v' = v/U_\infty$ and $\rho' = \rho/\rho_\infty$ where U_∞ and ρ_∞ is the velocity and density of the freestream respectively and L is a characteristic length, equation (8) can be written as,

$$u' \left(\frac{dc_O}{dx'} \right) + v' \left(\frac{dc_O}{dy'} \right) = \frac{K_1(\rho_\infty L)}{U_\infty} \rho' c_{O_2} c_M \quad (9)$$

where

$$K_1 = \frac{M_O}{M_{O_2} M_M} k_f \quad (10)$$

Equation (9) shows that for two steady flows with the same post-shock temperature, resulting in the same K_1 , and the same freestream velocity, the mass fraction distribution along the normalized directions x' and y' will be identical between the two flows if the product $\rho_\infty L$ is preserved. This is the statement of binary scaling. Also, from Hornung [2], for an ideal chemically reacting gas, the rate of dissociation R_D is

$$R_D = \rho T^n e^{-\frac{E}{kT}} (1 - \alpha) \quad (11)$$

and the rate of recombination R_R is

$$R_R = \frac{\rho^2 T^n \alpha^2}{\rho_d} \quad (12)$$

where ρ is the gas density, α is the mass fraction of the dissociated gas, T is the temperature, k is Boltzmann's constant, n is a dimensionless constant and ρ_d is the characteristic density of dissociation. From the above equations, the dissociation rate, which is a two body reaction, can be rewritten as,

$$R_D = \frac{d\alpha}{dt} = \frac{dc_O}{dt} = u \left(\frac{dc_O}{dx} \right) + v \left(\frac{dc_O}{dy} \right) \quad (13)$$

for steady flows. Then,

$$\frac{L}{U_\infty} R_D = u' \left(\frac{dc_O}{dx'} \right) + v' \left(\frac{dc_O}{dy'} \right) = \frac{(\rho_\infty L)}{U_\infty} \rho' T^n e^{-\frac{E}{kT}} (1 - \alpha) \quad (14)$$

where $1 - \alpha = c_{O_2}$. This is the same statement as given by equation (9). Accordingly, for the recombination reaction the scaling factor is $\rho_\infty^2 L$. It is interesting to note that de Crombrughe et al. [11] made the discovery that the binary scaling law is not only applicable for preserving the chemical nonequilibrium behaviour in shock layers but also maintain the same diffusion processes in binary scaled chemically reacting boundary layers, resulting in further applications in subsonic high enthalpy wind tunnels such as plasma tunnels.

The simulation strategy given by Hornung [2] for chemically reacting blunt body flows considering only dissociation reactions is therefore as follows,

$$Q = Q \left(U_\infty, \rho_\infty L, \alpha_\infty, \frac{T_w}{T_0} \right) \quad (15)$$

where α_∞ is the mass fraction of dissociated gas in the freestream. For strong bow shocks (usually from blunt bodies), the Mach number is omitted from the above equation due to the Mach number independence principle. Reynolds number is omitted because the post-shock Reynolds number is automatically satisfied when U_∞ and $\rho_\infty L$, is matched since the freestream static temperature has only a small influence on the post-shock temperature of a strong bow shock which is mainly influenced by U_∞ [12]. Consequently, besides the atomic mass fraction distributions, duplication of the parameters in equation (15) gives a simulation of the temperature field, viscosity, Prandtl number and the specific heat ratio in the flowfield after a bow shock, between experiment and flight. However, for more slender bodies where Mach number and real-gas effects are important the Mach number has also to be matched, which for static temperatures less than 2000 K subsequently results in a duplication of the freestream static temperature T_∞ and freestream Reynolds number [13].

It is important to note that some important portions of hypersonic blunt body flows cannot be described by the binary scaling law which is derived based on the assumption of no radiation coupling and purely binary reactions. From de Crombrugge et al. [14], when binary scaling is applied, the impact of non-binary chemistry causes the shock layer in the subscale test model to be hotter and less dissociated than in flight, while the strength of radiation coupling increases with the length-scale of the flow resulting in the subscale flow having less radiation coupling than in flight which subsequently leads to the laboratory shock layer containing a greater enthalpy than the shock layer in flight. Furthermore, it should be noted that the duplication of the freestream dissociation level α_∞ in equation (15) is very difficult because the production of high enthalpy flows in the wind tunnels often requires heating the test gas to temperatures high enough to cause significant thermochemical excitation which normally does not relax to equilibrium at the test section. In flight, the freestream dissociation level is practically zero which is not the case for high enthalpy wind tunnels. A finite freestream dissociation level leads to a reduced density jump across a shock resulting in a larger shock stand-off distance [15]. Also, F_q from equation (1) is omitted in equation (15) because the flow quality that can be achieved in current real gas simulation facilities is only very low [2]. Consequently, these facilities are only used for investigations of effects that are less subtle than those that depend sensitively on F_q . Unfortunately, there are actually a number of important effects which do depend sensitively on F_q [2]. So, Lawson and Austin are currently investigating new ways to generate low-disturbance, high-enthalpy test flows [16]. It has to be mentioned that the flow quality in high enthalpy facilities strongly depends on the test condition. A good flow quality can be achieved, for example, in shock tunnels at low unit Reynolds numbers even at high enthalpies as it is proven by numerous heat flux measurements.

2.2. Airbreathing propulsion testing

In hypersonics, scramjets are of main interest as airbreathing propulsion systems. Therefore, the following considerations are focused on scramjet testing. Scramjet propulsion becomes of interest at speeds greater than 1.5 km/s. At these speeds and higher, there is a strong coupling between the external vehicle flowfield and the internal flow of the engine. Therefore, and due to other reasons, scramjet testing requires a sophisticated ground testing methodology.

From Stalker [1], ground simulation of scramjets involves producing the conditions which will allow the combustion process to reach the same degree of completion as in the equivalent flight configuration. One of the most popular scaling laws for scramjets is the pL-scaling, which was first stated by Stewart [17], where p is the static pressure and L is the characteristic length. The pL-scaling law states that, given that fuel distribution and heat transfer similarity is achieved in the scramjet, the scramjet combustor performance would scale with the factor pL [18].

So, if the inlet static temperature, inlet flow velocity and fuel-air mixture fractions (equivalence ratio), and hence the Mach number, ratio of specific heats and total enthalpy, are reproduced in the subscale test, duplicating the pL factor between experiment and flight, which also duplicates the Reynolds number, would result in a representative simulation of the flight scramjet combustion flow [19].

An experimental investigation carried out by Pulsonetti and Stalker [18] into the validity of the pL -scaling law showed that the ignition time, generally defined as the time for the temperature rise to reach 5% of the complete reaction temperature rise for a given temperature is proportional to one over pressure. The pL -scaling law is physically consistent because the ignition reaction which produces the free radicals responsible for initiating the reaction system is a two body reaction. They also mentioned that the wall boundary layer and viscous effects on the inside surface of the scramjet duct also scales with the pL law because for fixed Mach number and wall temperature ratio the boundary layer thickness, the displacement thickness and the momentum thickness are functions of the Reynolds number. Pulsonetti and Stalker also showed that the pL -scaling law works for scaling the mixing efficiency, which measures the completeness of mixing, and other mixing effects for normal or tangential fuel injections. The scaling of the heat transfer, in terms of Stanton number, was shown to obey the pressure length scaling reasonably well as long as the boundary layer for the wind tunnel model or the flight vehicle does not become transitional [20]. Furthermore, as long as the scaled pressure distribution in the combustion duct and consequently in the expansion nozzle is duplicated, which is achieved well in most cases by the pL scaling law [21], pL scaling preserves the thrust coefficient between scramjets of different scale. This can be shown as follows; given that the pressure distribution in the scramjet nozzle, which depends on the location x and y , is

$$p_n = f(x, y) \quad (16)$$

and the thrust coefficient is defined as,

$$C_\tau = \frac{2\tau}{A_i p_\infty U_\infty^2} \approx \frac{2\tau}{A_i p_{0,\infty}} f(M_\infty) \quad (17)$$

where τ is the thrust, A_i is a reference area and $p_{0,\infty}$ is the total pressure. Neglecting viscous forces, the thrust for scramjet 2, which is a scaled model of scramjet 1, can be expressed as

$$\tau_2 = \int p_1 \frac{L_1}{L_2} dA_2 \quad (18)$$

where A is the internal local flow cross-sectional area and L is the characteristic length of the scramjets. Since

$$dA_2 = \left(\frac{L_2}{L_1}\right)^2 dA_1 \quad (19)$$

equation (18) becomes

$$\tau_2 \frac{L_1}{L_2} = \int p_1 dA_1 = \tau_1 \quad (20)$$

Using equation (17), for same Mach numbers this equation becomes,

$$C_{\tau,2} A_{i,2} p_{0,2} \frac{L_1}{L_2} = C_{\tau,1} A_{i,1} p_{0,1} \quad (21)$$

which can be simplified to,

$$C_{\tau,2} p_{0,2} L_2 = C_{\tau,1} p_{0,1} L_1 \quad (22)$$

Since,

$$\frac{p_0}{p} = \left(1 + \frac{\gamma - 1}{2} M^2\right)^{\frac{\gamma}{\gamma - 1}} \quad (23)$$

and in case both Mach number and γ are maintained between the two

scramjet flows, equation (22) demonstrates that preserving the pL product preserves the thrust coefficient of the scramjets given that the scaled pressure distributions are duplicated.

Nevertheless, there are limitations to the pL -scaling law. The pL -scaling law is valid for scaling the combustion reaction time if the process is dominated by binary reactions. However, if three body reactions are significant and the combustion occurs under chemical nonequilibrium, which is not uncommon in subscale scramjets as shown by Karl et al. [19], the pL -scaling law would not hold. Karl et al. [19] showed that in small subscale scramjet testing at subsequently high static pressures, maintaining the pL factor, which consequently preserved the Reynolds number, often did not preserve the chemistry (Damköhler's first number) which scaled better with $p^{1.7}L$. Consequently, in these cases it would be impossible to duplicate both the Reynolds number and the chemical time scales simultaneously. As demonstrated by Pulsonetti and Stalker [18], a consequence of incorrectly simulating the nonequilibrium combustion chemistry could be that the final pressure achieved in the scramjet prior to the nozzle expansion is scaled incorrectly which would then influence the thrust produced. Furthermore, the pL -scaling law does not preserve the equilibrium composition. Therefore, under chemical equilibrium conditions, the static pressure changes would impact the amount of heat released due to combustion since more molecular species would form at high pressures which would result in larger energy releases [18]. Nevertheless, while the pL -scaling law may not work so well in certain cases, it is still regarded as a good first order approximation for scaling scramjet performances in most cases because the law provides a relation for predicting the fundamental phenomena occurring in a scramjet combustor [18,21,22]. Consequently, Karl et al. [19] mentioned the importance of the use of CFD tools to relate data from pL scaled scramjet experiments to flight scale scramjets.

3. Types of hypersonic ground test facilities

To carry out hypersonic ground test experiments, a variety of different facilities exist. The facilities have different characteristics as shown in Fig. 3 and Fig. 4 as well as in Table 1. Shock tunnels and expansion tunnels can generate conditions with very high velocities, but

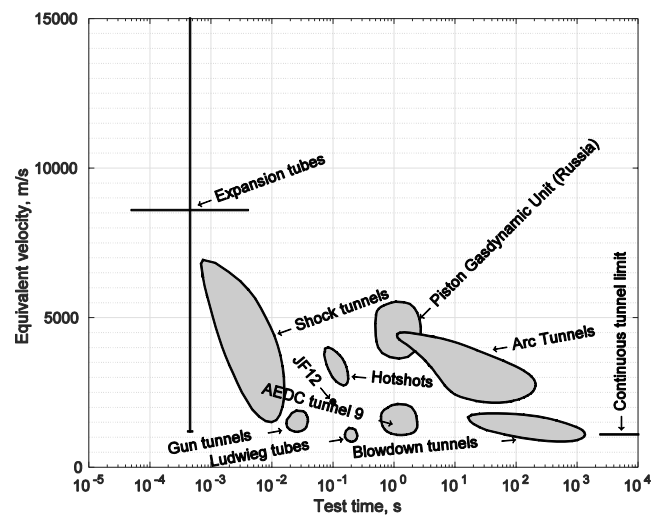


Fig. 4. The ranges of velocity and test time for different facility categories assuming air as test gas. Adapted from Ref. [52].

these facilities have very short test times. For example, the test time of expansion tubes in Table 1 are in the order of tens of microseconds. On the other hand, blowdown tunnels, Ludwieg tubes, hotshots and gun tunnels have long test times but are limited to producing low velocity conditions. The test times of gun tunnels and hotshots in Table 1 are in the order of tens of milliseconds, while the test times of blowdown tunnels are in the order of a few seconds, but within this group only hotshots can generate total temperatures of up to 6000 K. Conventionally driven reflected shock tunnels have medium duration test times (in the order of a few milliseconds) and medium performance capabilities compared to the other facilities. The biggest hypersonic wind tunnel currently in operation is the JF12 reflected shock tunnel which has a test section diameter of 2.5 m [23]. The LENS XX expansion tunnel comes close with a test section diameter of 2.4 m [24]. Though, it should be

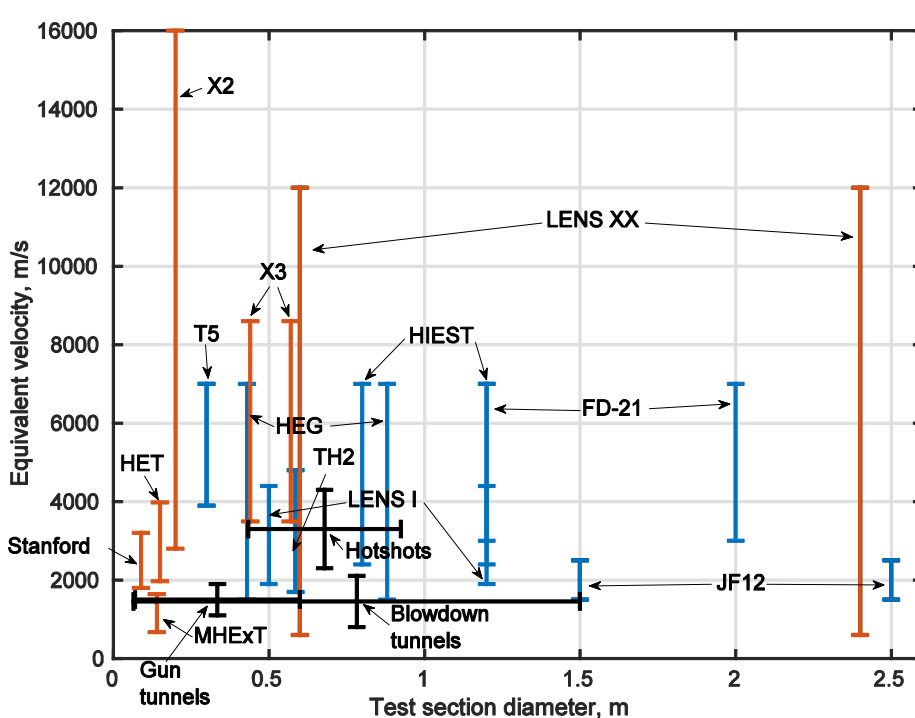


Fig. 3. The ranges of velocity and test section size for different facility categories assuming air as test gas. Expansion tubes are in blue, shock tunnels are in orange and other facilities are in black. (For interpretation of the references to colour in this figure legend, the reader is referred to the Web version of this article.)

Table 1

Characteristics of some existing hypersonic test facilities.

Facility type	Facilities	P _{0,max} , MPa	T _{0,max} , K	Typical test time	Test section diameter, m	Source
Continuous	AEDC Tunnel B	6.2	750	–	1.27	[25]
	AEDC Tunnel C	14	1200	–	1.27	[25]
Blowdown	AEDC Tunnel 9	145	1600	0.23 s–15 s	1.5	[26]
	H2K	4.5	1100	Up to 30 s	0.6	[27]
Gun tunnels	S4 Modane	15	1800	25–90 s	0.7–1.0	[28]
	Longshot, VKI	400	2500	20 ms	0.36–0.60	[29]
	Cranfield University	10	1290	80 ms	0.2	[30]
	HS1	60	1150	20 ms	0.6	[30]
Adiabatic compression unit	Oxford University	9	1000	30 ms	0.21	[30,31]
	AT-303	300	2500	50 ms–200 ms	0.3–0.6	[32]
Hotshot	ONERA F4	76	6000	20 ms–100 ms	0.43–0.92	[33,34]
Reflected shock tunnels	TH2	63	7400	2 ms–10 ms	0.586	[35]
	JF12	3.5	2500	100 ms–150 ms	1.5–2.5	[23]
	T4	90	7540	0.5 ms–5 ms	0.135–0.375	[36–38]
	T5	85	10000	1 ms–2 ms	0.3	[36,39]
	HEG	90	9900	1 ms–6 ms	0.43–0.88	[36]
	HIEST	150	10000	More than 2 ms	0.8–1.2	[40]
	FD-21	–	10000	–	1.2–2	[41,42]
	LENS I	200	7000	2 ms–18 ms	0.5–1.2	[43–45]
	MHEXT	1.4	2000	900 μs–1000 μs	0.14	[46]
	Stanford University	3.3	4188	170 μs–400 μs	0.089	[47]
Expansion tunnels	HET	53	5400	90 μs–150 μs	0.15	[48]
	X2	19700	37000	50 μs–200 μs	0.2	[22,49]
	X3	27500	18200	300 μs–1300 μs	0.44–0.57	[50,51]
	LENS XX	–	0.6–12 km/s	200 μs–8000 μs	0.6–2.4	[24]

noted that, in general, the test section size of expansion tunnels is much smaller than that of the LENS XX. It has also to be noted that, the test section size is not necessarily a measure of the reasonable model size. This topic is discussed in detail in section 4.2.1.

Nevertheless, it is not always desirable to test in facilities as big as possible. The advantage of having smaller facilities is the economy of operation and cost. It is also not always necessary to produce very high velocity conditions, for example in scramjet testing. Similarly, long test times may not be necessary for the study of thermochemical kinetics. Thus, different facilities are suited for different objectives. The characteristics of some of the popular facility types will be covered in this section.

3.1. Low enthalpy facilities

Under low enthalpy hypersonic conditions, approximately less than 2 MJ/kg, the gas behaves like a perfect gas and the Mach-Reynolds-Simulation is valid. For investigating low enthalpy conditions, adiabatic compression units, blowdown tunnels and gun tunnels are all suitable facilities, but for the sake of brevity adiabatic compression units are omitted here as these facilities are uncommon.

A schematic of a conventional blowdown tunnel is shown in Fig. 5. The flow condition at the test section depends on the pressure and temperature of the test gas in the plenum. Initially during the operation of a blowdown tunnel, the nozzle and test section are evacuated to low pressures and isolated from the plenum. Gas from the high-pressure tank

is used to pressurize the plenum. In the AEDC tunnel 9 blowdown facility, heaters are used to heat the fixed volume of pressurized test gas in the plenum to a particular pressure and temperature to create hypersonic conditions at the test section [26]. Once the gas in the plenum reaches the desired pressure and temperature, the diaphragm will rupture. The high pressure and temperature test gas will then expand through the nozzle resulting in a limited duration of hypersonic flow. As the high temperature and high pressure test gas leaves the plenum, high pressure gas from the high-pressure tank enters the plenum from the upstream end. This process is organized such that the cold gas from the high-pressure tank pushes the heated test gas downstream like a piston to maintain a constant nozzle inlet condition. Instead of a diaphragm, other facilities like H2K use a valve in front of the plenum chamber to connect the wind tunnel with the high-pressure reservoir and electric heaters placed upstream of the settling chamber and the valve [27].

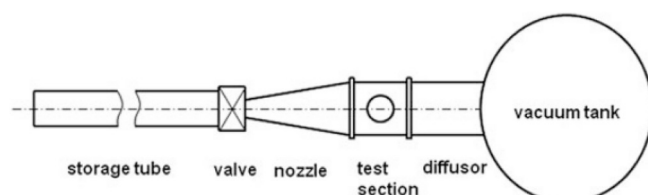


Fig. 6. Schematic diagram of a Ludwieg tube [53].

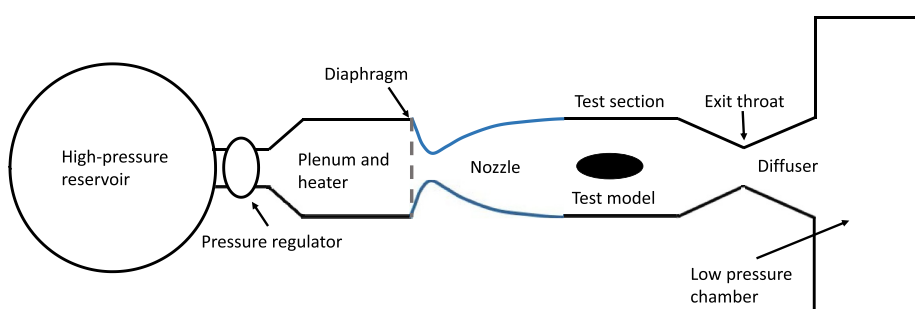


Fig. 5. Schematic diagram of a blowdown wind tunnel like the AEDC Tunnel 9.

A different form of a blowdown tunnel is the Ludwieg tube, shown in Fig. 6, where upstream of the nozzle is a long tube containing high pressure test gas which is sometimes also heated. Once the diaphragm or valve separating the nozzle and high pressure tube opens and the test begins, an unsteady expansion forms. A large part of the expansion wave propagates upstream through the high pressure tube, reflecting off the end wall and back to the nozzle entrance. Once the first reflected expansion wave arrives back to the nozzle entrance, the test is terminated. During the upstream and downstream movement of the expansion wave, the conditions in the nozzle reservoir are at least theoretically constant which is an advantage of Ludwieg tubes. Generally, for blowdown facilities the reservoir pressure is not constant with time because of the constant volume of the high-pressure reservoir. This leads to the fact that for constant volume reservoirs, the Reynolds number and other flow parameters decrease during the measuring time.

Another form of a blowdown tunnel are hotshots, where upstream of the nozzle is an arc chamber. The arc chamber is filled with the test gas. The test gas is then heated by an electric arc, creating a high pressure and high temperature reservoir for the nozzle inlet.

Another way to create high pressure and high temperature nozzle inlet reservoirs is to compress the test gas using a light free piston. Facilities operating in this way are known as gun tunnels, shown in Fig. 7. To operate the gun tunnel, the driver section is pressurized and the barrel section is filled with the test gas. Once the primary diaphragm ruptures, the piston is pushed downstream through the barrel by the high pressure driver gas and compresses the test gas. A shock wave forms in front of the piston and propagates down the barrel at a higher velocity than the piston. The shock wave will reflect off of the end of the barrel and the secondary diaphragm will rupture. The shock wave will reflect between the upstream face of the piston and the end of the barrel multiple times as the piston travels downstream. As the piston travels downstream, it will decelerate as the test gas pressure increases. Eventually the piston will stop and a peak in test gas pressure in the barrel will be reached. In the case of the Longshot gun tunnel, as the peak pressure is reached, a system of valves at the downstream end of the barrel closes, trapping a high pressure and high temperature reservoir for the nozzle inlet [54]. In this case, the fixed volume reservoir will not be influenced by the motion of the piston as it rebounds upstream and this prolongs the test time.

3.2. High enthalpy facilities

Under high enthalpy conditions where the velocity is around 2–7 km/s, real-gas effects such as vibrational excitation and chemical reactions like dissociation and recombination occur behind strong shocks (created by blunt bodies for example). For these kinds of blunt body flows, the Mach number becomes irrelevant while the freestream density and velocity become important simulation parameters. To create these high enthalpy conditions, higher pressure and temperature reservoirs are required at the inlet of a convergent-divergent nozzle compared to those found in low enthalpy facilities. This can be achieved by driving a strong shock wave through a tube filled with test gas while having a small enough nozzle throat, which at the beginning is closed by a secondary diaphragm, such that a reflected shock forms to create a stagnated nozzle inlet reservoir. These facilities are known as reflected shock tunnels, shown in Fig. 8. In most cases, the test time terminates when the driver gas arrives at the test section and this topic is discussed

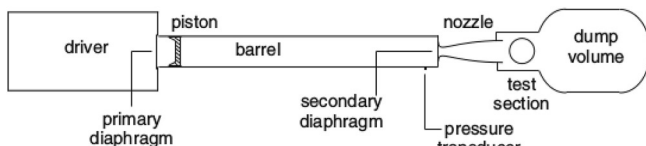


Fig. 7. Schematic diagram of a gun tunnel [30].

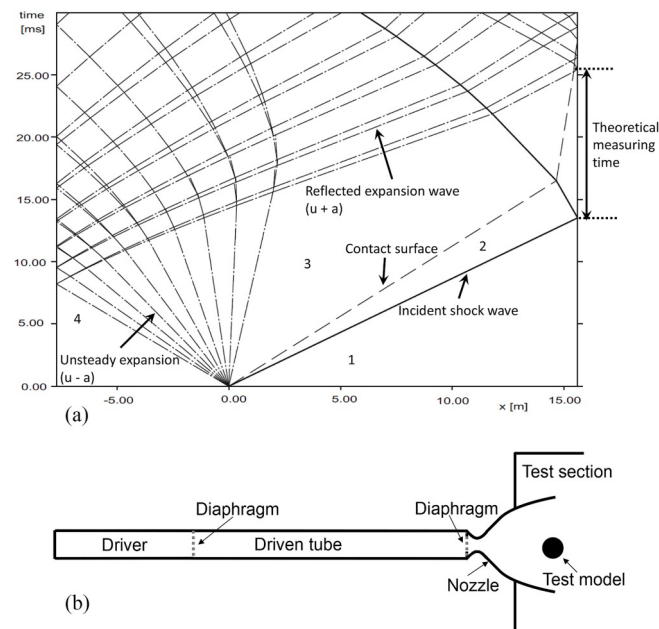


Fig. 8. Wave diagram (a) and schematic (b) of a reflected tunnel.

in detail in section 4.2.1. Hotshot facilities are also capable of producing high enthalpy conditions, but are omitted here for the sake of brevity as these facilities are less common.

When the primary diaphragm ruptures, for given filling conditions in the driven tube the speed of the shock wave formed in the shock tube depends on the initial driver gas pressure and driver gas speed of sound, which consequently depends on the temperature and chemical composition. This relationship is shown in Fig. 9 for a pure helium driver assuming calorically perfect and thermochemical equilibrium gas, where the equilibrium results were computed using the PITOT code [55] simulating a free piston driver. From Fig. 9, one of the results is that high temperature real gas effects decrease the shock speed. It is also important to note that the driver section often has a larger diameter than the shock (driven) tube. In this case, after diaphragm rupture for a free piston driver, the driver gas undergoes a steady expansion to a choked throat condition, $M = 1$, before an unsteady expansion into the driven section [55], provided the driver gas behind the contact surface reaches supersonic speed. This is done for improved performance, as can be observed in Fig. 9 with shock speed improvements of around 20%, because a steady expansion provides a higher velocity increase in subsonic flow than an unsteady expansion for a given pressure difference [56,57]. Furthermore, one of the most important result in Fig. 9 is that for a given driver gas at high pressure ratios, an increase of its temperature is much more effective than an increase of its pressure, concerning a gain in shock speed. As a matter of fact, at infinitely large pressure ratios, p_4/p_1 (refer to Fig. 8 (a) for definition of the subscripts), the shock speed U_s approaches the finite value,

$$U_s = \frac{\gamma_1 + 1}{\gamma_4 - 1} a_4 \quad (24)$$

where a_4 and γ_4 is the speed of sound and ratio of specific heats of the driver gas respectively, assuming calorically perfect gas. In this aspect, it is desirable to select a driver gas with a low molecular weight, resulting in a naturally high speed of sound at a given temperature, for use as the driver gas. Consequently, helium and hydrogen are popular driver gases. Using electrical resistance heaters, helium and hydrogen can be heated up to 800 K [58]. Assuming air as the test gas, $a_4/a_1 \approx 4.8$ and $a_4/a_1 \approx 6.2$ can be obtained using heated helium and hydrogen respectively. From heated helium, the TH2 reflected shock tunnel could produce a nozzle exit velocity of up to 3.6 km/s while, from heated hydrogen, the

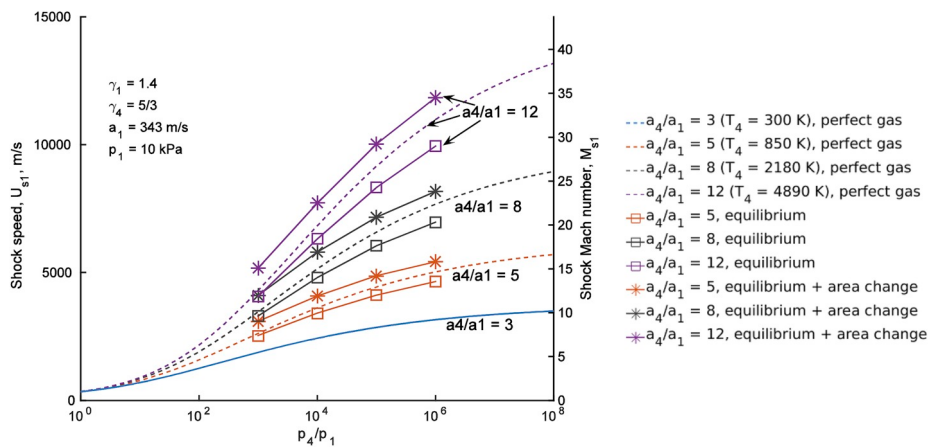


Fig. 9. Relationship of shock speed and pressure ratio between the driver pressure, p_4 , and test gas fill pressure, p_1 , with different speed of sound ratios between the driver, a_4 , and test gas, a_1 , for a pure helium driver.

LENS I reflected shock tunnel could produce a nozzle exit velocity of up to 5.0 km/s [44]. However, to produce velocities greater than 4–5 km/s, it is necessary to use other methods which allow the driver gas to be heated beyond 800 K as it is unsafe, expensive and inefficient to use very high driver pressures for performance gains. In fact, for a given a_4/a_1 , it is impossible to attain certain shock speeds regardless of how high the driver pressure is because the shock speeds effectively asymptote as shown in Fig. 9 and by equation (24).

One way to achieve very high driver gas temperatures is heating the driver gas with an electric discharge. Such drivers are known as electric arc drivers and can heat helium to 20000 K resulting in $a_4/a_1 \approx 24$ [59]. This driver method is used for the 10 cm inner diameter shock tube facility EAST (Electric Arc Shock Tube) at the NASA Ames Research Centre, which can also run as a shock tunnel [60]. When operated as a reflected shock tunnel, total specific enthalpies of more than 30 MJ/kg could be achieved. However, the total pressures corresponding to these high enthalpy conditions were less than 20 MPa [58]. Consequently, while there is no doubt that electric arc heating can generate very high temperature driver gas, it remains to be seen whether high temperature test gas can be produced at high pressures necessary for high total pressure operation.

Another way to achieve high heating of the driver gas is to compress the gas almost adiabatically, and virtually isentropically [61,62], with a heavy free piston. This method was first reported by Stalker and Besant in 1959 [63] and is currently used in various reflected shock tunnels around the world, including HEG in Germany, HIEST in Japan, T5 in the USA and T4 in Australia [36] and others. These free piston driven shock tunnels are known as Stalker tunnels, named after the pioneer of the free piston driver. Helium is normally used as the driver gas for free piston drivers. A certain amount of argon is sometimes mixed with helium to control the performance of the free piston drivers. The driver gas typically gets compressed to pressures in the range of tens to the low hundreds of MPa when the diaphragm ruptures [62,64]. Values of $a_4/a_1 \approx 12$ can be achieved in free piston drivers [65,66], as is demonstrated by the free piston driver of HEG, T4 and T5 which heats helium driver gas to over 4000 K [64]. The largest Stalker tunnel currently in regular operation is HIEST with a test section diameter of up to 1.2 m [40]. A new Stalker tunnel, FD21, is currently being put into operation in China and would become the biggest Stalker tunnel in the world, having a test section diameter of 2.0 m and a total length of more than 110 m [41].

A third way to heat helium driver gas is to add a certain amount of hydrogen-oxygen, for example, with the helium driver and this allows the use of deflagrative combustion to heat the driver gas mixture. The optimum helium content for performance, is about 50–80% by volume [67]. While the combustion process allows the gas mixture to be heated to about 2500 K, the amount of water vapour formed from combustion

increases the average molecular weight of the driver mixture. As a result, this driver method can produce $a_4/a_1 \approx 7\text{--}8$. Currently, no hypersonic facility in operation utilizes this deflagrative combustion driver method. The issue with this method is that the post-combustion pressure is limited to about 40 MPa due to the need to suppress detonation. Consequently, detonative combustion methods have been developed to overcome the pressure limitation of the deflagrative combustion method. For the detonation driver, the optimum helium content for performance, is about 30–60% by volume and this can result in $a_4/a_1 \approx 7\text{--}8$ [67]. So the performance characteristics of the detonation driver is similar to that of the deflagrative driver except detonation drivers allow for higher driver pressures to be attained. Currently operating detonation driven shock tunnels include TH2 in Germany and JF12 in China [68].

Compared to the free piston driver, the clear disadvantage of the detonation driver is the inferior performance. Furtheron, the storage and handling of hydrogen requires safety precautions. After each experiment the water as product of the detonation combustion has to be removed off the facility by evacuation or other means. This limits the number of shots within a certain period of time. Nevertheless, detonation drivers are sometimes selected over free piston drivers due to its low cost. Free piston drivers are much more expensive. Also, free piston drivers are much more complex in their mechanical setup and therefore require much more experience in operation. Detonation drivers do not need any complex mechanical systems and therefore are much easier to operate than free piston drivers. Hence, detonation drivers allow for a convenient performance upgrade from a conventional helium/hydrogen driven shock tunnel without significant hardware modification. An example of a facility doing such an upgrade is the TH2 [70] reflected shock tunnel.

In a reflected shock tunnel, three different processes can occur in the shock tube when the reflected shock wave meets the constant surface. This is illustrated in Fig. 10. In the undertailored operation, the shock wave interaction with the contact surface causes a transmitted shock and a reflected expansion wave that propagates towards the end of the shock tube. In the overtailored operation, a transmitted shock as well as a shock wave which reflects off the contact surface is generated. In this case, behind the first interaction the contact surface continues to travel downstream while reflected shock waves travel back and forth between the contact surface and the end of the tube. In the tailored operation, the reflected shock wave travels through the contact surface and, in case of a closed shock tube, reduces the velocity of the contact surface to zero. In this case, no further expansion waves or reflected shock waves are formed. Generally, the tailored operation is the most desirable form as it allows for a steady nozzle reservoir state and a long test time. Furtheron, it results in a reduced driver gas contamination of the test gas (see

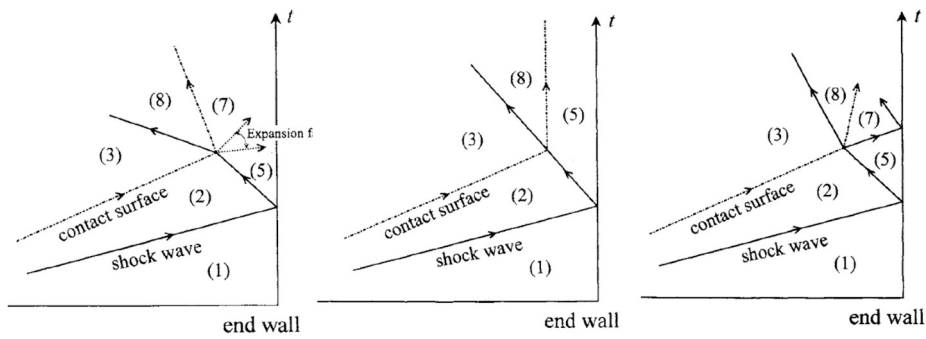


Fig. 10. x-t wave diagrams of shock wave/contact surface interactions for undertailored (left), tailored (middle) and overtailored (right) configurations. Dashed lines represent contact surfaces while solid lines represent shock waves [69].

section 4.2.1) because in this case there is only one interaction of the reflected shock with the contact surface. In case of an overtailored operation the multiple reflections of the shock at the contact surface cause the generation of a new driver gas wall jet with each reflection. Therefore, driver gas contamination is a serious concern for overtailored operation. For the undertailored mode, during the first shock-contact surface interaction, the reflected expansion wave accelerates the hot test gas away from the nozzle entrance and therefore the velocity of the driver gas wall jet is at least decelerated which leads to a reduced driver gas contamination. Therefore, in respect to driver gas contamination a slight undertailored operation is desirable.

For a given driver condition, a tailored operating condition can only be obtained for a unique driven section filling condition and vice versa. Using the methodology outlined by Nishida [69] and assuming inviscid, calorically perfect gas, the driver conditions necessary for tailored operation and the resulting shock speeds were calculated for different driver gases given that the test gas initially filled in the shock tube is air at room temperature. The results are presented in Fig. 11. This figure should only give qualitatively an estimation of the magnitude of the shown parameters since the assumption of a calorically perfect gas is not valid for the shown high driver gas temperatures and shock speeds. Because of the requirement of tailored operation, it is not so convenient to vary the shock speed which could otherwise be done by varying the driver gas temperature and the ratio of driver pressure, p_4 , to driven section fill pressure, p_1 , to any arbitrary combination. As an example from the results in Fig. 11, to generate a 6 km/s shock in room temperature air using a helium driver, the driver needs to have a temperature of around 6300 K and a pressure of around $3000p_1$ for tailored operation. If the facility cannot heat helium to 6300 K, compensating by increasing the value of p_4/p_1 is not an option as it would result in untailored interface conditions. Instead, a solution could be to use hydrogen as the driver gas as it would produce a 6 km/s shock when

heated to only around 2200 K. Hence, as mentioned by Lukasiewicz [57], operation of reflected shock tunnels often involves using different types of driver gas conditions and driver gas mixtures to maintain tailored interface configurations at different total enthalpy test conditions. Nevertheless, from Olivier [35], Marineau et al. [71] and Sudani et al. [72], operating reflected shock tunnels at slightly off-tailored conditions may still be acceptable. In particular, operating at a slightly undertailored condition is even recommended by Sudani et al. [72] for improved test time at the cost of a slightly less steady nozzle exit condition. However, operating overtailored should always be avoided due to pronounced driver gas contamination on top of a less steady nozzle exit condition [37,72,73].

Assuming a tailored interface, the ratio of nozzle reservoir pressure, p_5 , to driver pressure, p_4 , for different shock speed conditions are calculated assuming as above inviscid, calorically perfect gas and in the same way as Nishida [69]. The ratio p_5/p_4 is often called the pressure recovery factor or the recovered pressure. The results are presented in Fig. 12 and they show that the driver pressure, p_4 , needs to be of a comparable value to the desired total pressure of the test condition as the pressure recovery factor is about 0.9 for most conditions. Similarly, for a free piston helium driver, Stalker and Hornung [74] calculated the pressure recovery factor for air as test gas to be about 1.8 under tailored interface operation in the case of an area change at the driver-shock tube junction. With the influence of real gas effects, p_4 should still be in the same order of magnitude as the desired total pressure of the test flow under tailored conditions. This means that the value of p_4 , and consequently p_1 due to Fig. 12, cannot be arbitrary if a test condition with a particular total pressure is desired. For example, if heated helium is used as the driver gas and a test condition with a total pressure in the hundreds of MPa is required, then p_4 also needs to have a value in the hundreds of MPa while p_1 needs to have a value around the hundreds of kPa. Also, from Figs. 11 and 12, it can be observed that the total pressure

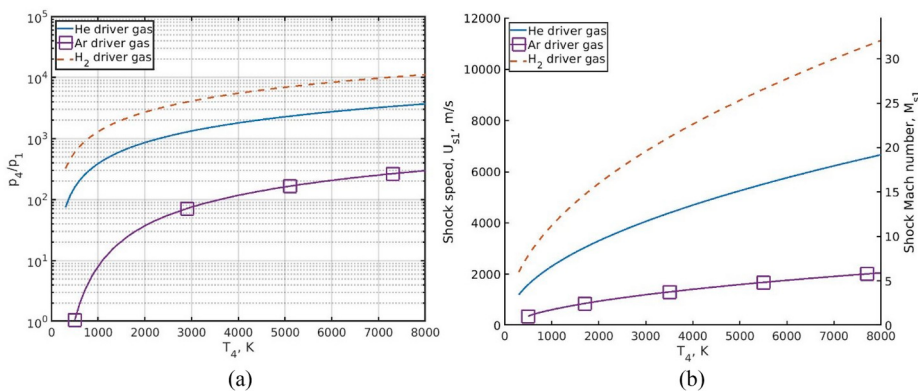


Fig. 11. The ratio of driver pressure, p_4 , to driven section fill pressure, p_1 , (a) and the shock speed, U_{s1} , (b) for tailored operation at various driver gas temperatures, T_4' , for a test gas of air initially at room temperature and three different driver gases.

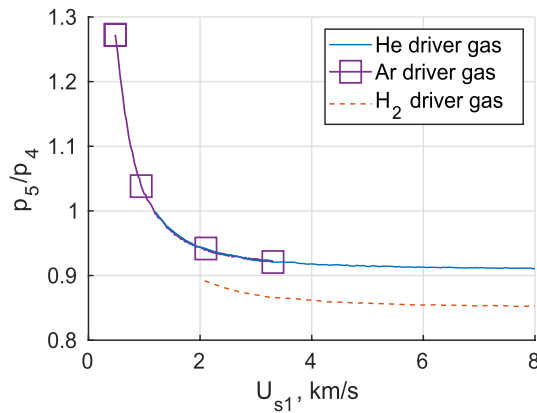


Fig. 12. The ratio of nozzle reservoir pressure, p_5 , to driver pressure, p_4 , versus shock speed, U_{s1} , for tailored operation given a test gas of air initially at room temperature and three different driver gases.

of the test conditions can be varied without influencing the shock speed while operating under tailored interface conditions.

Consider a representative high performance free piston driver heating helium to around 5000 K, a shock Mach number, M_{s1} , of 15 is produced for tailored operation in a reflected shock tunnel as shown in Fig. 13 (a). It has to be noted that the graph shown in Fig. 13 (a) has been determined for calorically perfect gas since the underlying theory is only valid for calorically perfect gas. Fig. 13 (b) and (c) show the nozzle reservoir conditions for a range of M_{s1} at typical shock tunnel fill pressures of air assuming thermochemical equilibrium. All thermochemical equilibrium calculations reported in this paper were performed using the CEA code of NASA [75]. Given $M_{s1} = 15$, the resulting nozzle reservoir condition is, $p_5 \approx 3.4\text{--}340$ MPa for the given initial pressure, $T_5 \approx 8800\text{--}11700$ K and $h_5 \approx 28$ MJ/kg. The currently operational

reflected shock tunnels generally do not operate above these conditions. The performance of reflected shock tunnels is generally limited to about 7 km/s for nozzle exit velocity, 25 MJ/kg for total enthalpy, 10000 K for total temperature and 200 MPa for total pressure [67]. However, the main contributor to this performance limitation is generally not from driver capabilities as modern impulse facility drivers, particularly free piston drivers, have the potential of supporting higher velocity and total pressure conditions. The performance limitation of reflected shock tunnels mainly arises from the current material limitations leading to erosion and nozzle throat melting (see section 4.2.2). Furthermore, the influence of premature arrival of driver gas at the test section increases with increasing shock velocity resulting in almost no test time beyond 7 km/s (25 MJ/kg) for the case of the T3 [61] and T5 [65] reflected shock tunnels. Also, the possibility of significant radiation loss by the nozzle reservoir at high total enthalpies could make reflected shock tunnels inefficient facilities for producing very high enthalpy flows.

3.3. Very high enthalpy facilities

So far, all the facilities discussed involves expansion of a stagnated gas through a converging-diverging nozzle. However, in order to generate conditions with higher total pressures and total temperatures, it is necessary to not stagnate the test gas. In this way, one such facility which allows high enthalpy conditions is the non-reflected shock tunnel. This facility is almost identical to a reflected shock tunnel except the nozzle is a purely diverging nozzle because the test gas does not stagnate at the end of the shock tube but, instead, travels “straight-through”. While non-reflected shock tunnels allow for higher performance, the test time of a shock tunnel in non-reflected mode is always significantly less than its test time in reflected mode [58]. There are currently no non-reflected shock tunnels in operation.

Another facility which can be used to produce high enthalpy conditions is the expansion tube, shown in Fig. 14, which was first proposed

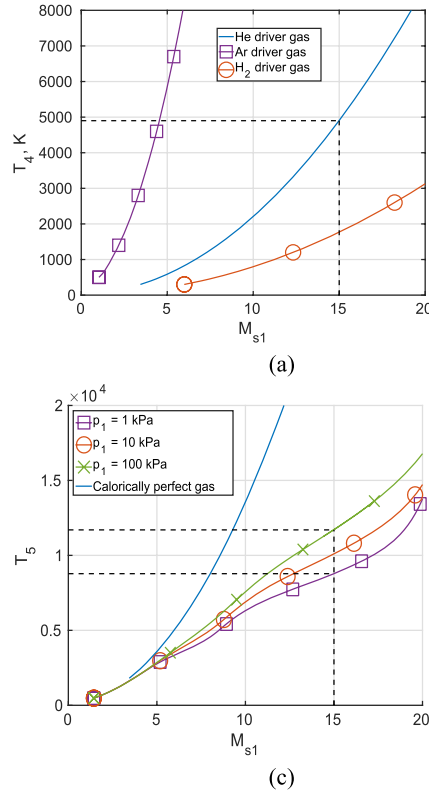


Fig. 13. Driver temperature, T_4 , versus shock Mach number, M_{s1} , for tailored operation for (a) calorically perfect gas. Figures (b), (c) and (d) show the relationship of the nozzle reservoir pressure, p_5 , temperature, T_5 , and enthalpy, h_5 , respectively with M_{s1} for both thermochemical equilibrium and calorically perfect gas.

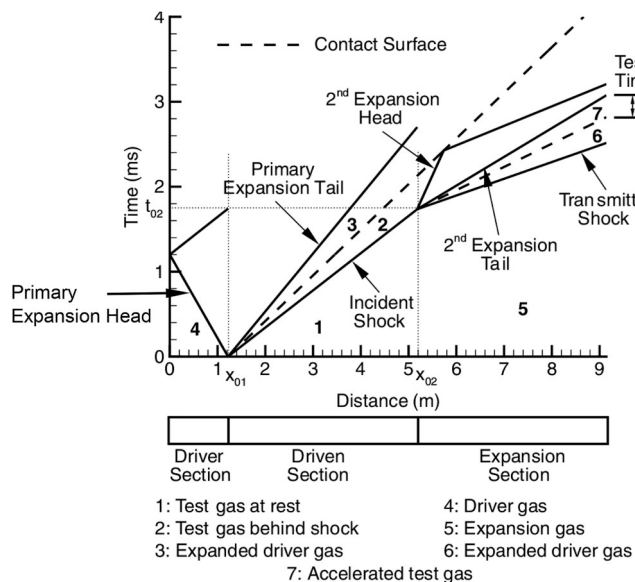


Fig. 14. Schematic and x-t diagram of an expansion tube showing the typical wave processes which occur during operation [48].

by Resler and Bloxsom in 1952 [76]. In the expansion tube, the shock tube is connected to an additional tube of the same inner diameter, called the acceleration tube, which is initially separated from the shock tube by a weak diaphragm and is evacuated to very low pressures. When an expansion tube experiment is initiated, a shock wave passes through the shock tube, shock heating the test gas and then breaking the secondary diaphragm when it reaches the end of the shock tube. An unsteady expansion forms after the rupture of the secondary diaphragm. The shock heated test gas travels through the unsteady expansion as it flows through the acceleration tube and this increases the total pressure and total enthalpy of the test gas. The unsteady expansion performs work by the time-dependent pressure force which according to the equation [57].

$$\frac{dh_0}{dt} = -\frac{1}{\rho} \frac{\partial p}{\partial t} \quad (25)$$

leads to a total enthalpy increase for part of the gas. As explained by Morgan [77], the unsteady expansion causes a total pressure and total enthalpy multiplication, the magnitude of which depends purely on the Mach number of the expanded test gas, M_7 (refer to Fig. 14 for definition of the subscripts), according to perfect gas analysis. This general trend is

also observed in thermochemical equilibrium analysis, shown in Fig. 15 and calculated using the PITOT code [55], where the relationship between M_7 and the magnitude of multiplication was calculated for an air test gas with a fill pressure of $p_1 = 10000$ Pa subjected to different shock speeds, $U_{s,1}$. For the range of M_7 shown, which is realistic for a typical expansion tube, the test gas total enthalpy and total pressure could increase by a factor of around 2–4 and 40–1000 respectively from its value after shock heating in the shock tube. Thus, for a given driver, the expansion tube can generally produce the highest total pressure and total enthalpy conditions of all the facilities.

One of the earliest operational expansion tubes was run by Miller [78] at NASA Langley in the 1970s. While the facility demonstrated its performance potential, it was decommissioned in 1983 because very few usable operating conditions could be produced due to severe noise in the test flow. Consequently, the expansion tube facility was not established as a reliable research tool until the early 1990s when Paull and Stalker [79] found a solution to inhibit the severe perturbation present in the test flow. The noise in the test flow was found to be acoustic disturbances transferred from the expanded driver gas, and the source of the noise in the driver gas was the primary diaphragm rupturing process. All frequency components of the acoustic disturbance in the test gas are focused into a narrow frequency bandwidth during the unsteady expansion causing significant noise during the test time. The noise in the test flow can be reduced by reducing the transmission of acoustic disturbances from the expanded driver gas to the test gas prior to the unsteady expansion of the test gas. This can be done by designing the test conditions such that the speed of sound in the shock processed test gas, a_2 , is at least 1.3 times larger than the speed of sound in the expanded driver gas, a_3 , as proposed by Morgan [77]. Meeting this requirement permits the contact surface to act like an acoustic buffer which attenuates the transmission of acoustic disturbances from the expanded driver gas to the test gas. Nowadays, Lawson and Austin [16] reports that it may even be possible to generate conditions in the expansion tube with freestream disturbances low enough for accurate boundary layer transition studies with real gas effects.

Expansion tubes can be fitted with divergent nozzles to operate as expansion tunnels. The expansion tunnel has a distinctly longer test time than the non-reflected shock tunnel and a significant reason for this is because the accelerator gas, instead of the test gas, is used for nozzle start-up, unlike in a shock tunnel where test gas is wasted on nozzle start-up. Nevertheless, the expansion tunnel still has a much shorter test time compared to a reflected shock tunnel of a similar size. Additionally, although expansion tubes can be operated with nozzles to provide an increase in the test section size (and a small increase in the test time), the area increase by expansion tunnel nozzles are much smaller than that by reflected shock tunnels. For example, the nozzle exit area to the shock

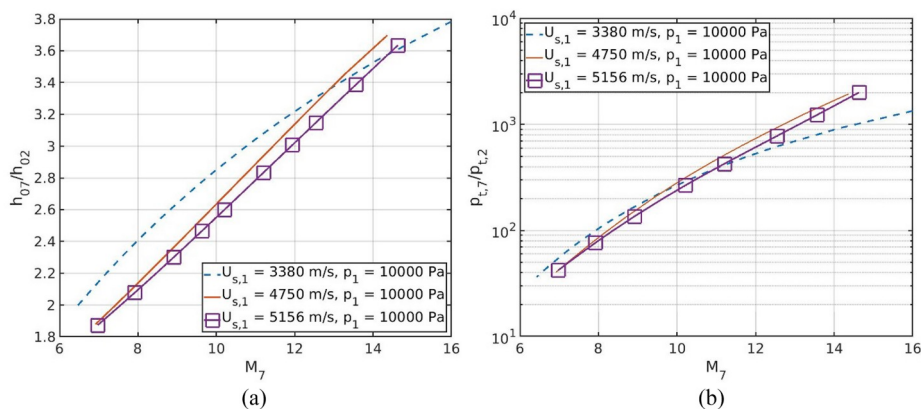


Fig. 15. Total enthalpy (left) and total pressure (right) gains across an unsteady expansion under thermochemical equilibrium conditions. h_{07} and $p_{t,7}$ refers to the total enthalpy and total pressure respectively of the test gas after unsteady expansion to a Mach number M_7 , h_{02} and $p_{t,2}$ refers to the total enthalpy and total pressure respectively of the test gas after shock heating by a shock with speed $U_{s,1}$ for a fill pressure of p_1 .

tube area of HEG nozzles ranges from 8:1 to 34:1 while the nozzle area ratio of the X2 expansion tunnel is only 5.64. Therefore, for a shock tube of the same diameter, a reflected shock tunnel would always have a much larger test section than an expansion tunnel.

The expansion tube and tunnel, however, are not exclusively used for generating high total pressure and/or total enthalpy conditions, as shown in Fig. 19 and Fig. 23. Expansion tubes such as the one at Stanford University [47] and the one at The University of Michigan (MHEXT) [46] operates low enthalpy test conditions for the study of combustion, while the X2 expansion tunnel operating with a conventional helium driver provides medium enthalpy conditions for the study of CO₂ thermochemical nonequilibrium and radiation [80]. Hence, while the reflected shock tunnel has significantly longer test times and allows for the use of larger test models than the expansion tube, the thermochemical state of the test flow generated by expansion tubes is more realistic of flight. This is because in a reflected shock tunnel, complete thermochemical equilibration is unlikely to occur through the nozzle expansion. So, as the test gas never stagnates in the expansion tube and the occurrence of the unsteady expansion provides a total enthalpy multiplication, the test gas does not reach as high of a temperature as would be required in a reflected shock tunnel to generate the same condition.

Assuming that the total enthalpy of the shock heated test gas is $h_{02} \approx U_{s,1}^2$ [58] which holds for high shock Mach numbers and assuming the total enthalpy of the test flow is $h_{0\infty} = 0.5U_\infty^2$, Fig. 16 is produced which illustrates the benefits of the total enthalpy multiplication occurring in expansion tubes. The figure shows that, given a required test section velocity, U_∞ , the shock speed, $U_{s,1}$, required to generate this test flow is significantly less in expansion tubes compared to reflected shock tunnels. For example, to generate a 4.0 km/s flow at the nozzle exit of a reflected shock tunnel, a shock tube shock speed of about 3.0 km/s is necessary and this would heat the test gas to a temperature of almost 6000 K after shock reflection, resulting in significant dissociation of the test gas. On the other hand, to generate the same condition in an expansion tube, a shock tube shock speed of only about 2.0 km/s is required, resulting in very little dissociation of the test gas. Therefore, for a given test condition, the one generated by an expansion tube will always be closer to thermochemical equilibrium compared to the one generated by a reflected shock tunnel. Furthermore, even for superorbital expansion tube conditions where significant dissociation occurs in the test gas by shock heating, some experimental results seem to indicate thermochemical equilibrium across the unsteady expansion [81].

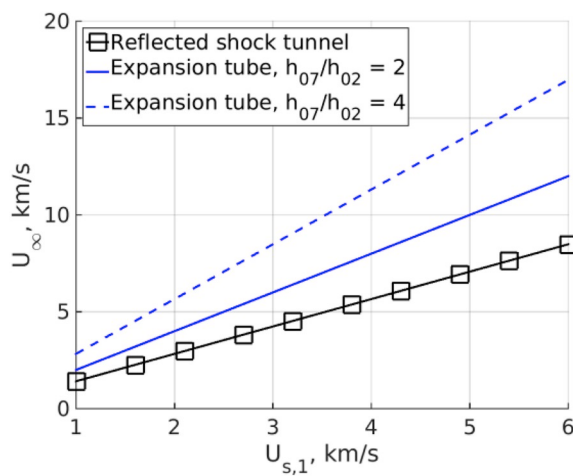


Fig. 16. An approximate relationship between the test section velocity and the shock speed required for reflected shock tunnels and expansion tubes.

4. Requirements and limitations of ground test facilities

The previous section introduced the characteristics of various different hypersonic ground test facilities. Now it is necessary to identify what is required of the facilities so that the capabilities and limitations of the current facilities can be recognized.

4.1. Performance requirements and limitations to simulate flight

As discussed in section 2, a significant portion of experimental work in hypersonics involves reproducing flows past actual aircrafts and spacecrafts for engineering purposes. Therefore, it is important to identify portions of flight trajectories which can and cannot be simulated by current ground test facilities. Some representative trajectories of typical flight vehicles are shown in Fig. 17 and these values are used for the analysis in this section.

An ideal ground testing would require the duplication of the real atmospheric and flight data. In order to recreate the Mach number, Reynolds number, ρ -L scaling, velocity and total enthalpy of a flight vehicle, it would be necessary to simultaneously recreate the chemical composition, freestream velocity, freestream static temperature and, in the case of using a full scale test model, the freestream static pressure/density of the flight condition – this is often not possible.

4.1.1. Low enthalpy flow regime

It is easy to show that full scale testing for hypersonic flow conditions is not feasible even for relatively low enthalpy conditions. Exemplarily, a wind tunnel of 5 m × 5 m cross-section simulating the flow conditions at 35 km altitude at Mach number 6 would require a theoretical driving power of 700 MW. Therefore, scaled model testing is the normal case. As shown in section 2.1.1, in low enthalpy flows no chemical reactions take place and therefore the gas can be considered as thermally perfect. In this flow regime the most important simulation requirements are given by the Mach number, the Reynolds number and for certain flow cases the wall temperature ratio. Depending on the considered flow phenomena, the freestream velocity may or may not be duplicated. The duplication of the flight velocity is of importance, for example, for full scale scramjet testing in order to simulate the correct travelling time of the flow through the engine. In case there is no need to duplicate the freestream velocity, this leads to some weaker requirements on the wind tunnel testing parameter as it is shown in the following. In this case only Mach and Reynolds number should be duplicated leading to the statement given in equation (1). The Reynolds number is given by,

$$Re = \frac{\rho_\infty U_\infty L}{\mu_\infty} \quad (26)$$

with

$$\rho_\infty = \rho_0^* f_1(\gamma, M_\infty) \quad (27)$$

$$U_\infty = a_\infty M_\infty = \sqrt{\gamma R \frac{T_\infty^*}{T_0^*}} \sqrt{T_0^* M_\infty} \quad (28)$$

$$U_\infty = \sqrt{T_0^*} f_2(\gamma, M_\infty) \quad (29)$$

and the usual approximation for the viscosity

$$\mu_\infty = C^* T_\infty^n \quad (30)$$

where the subscript 0 refers to the isentropic total conditions and C is a constant. With this and the equation of state for the reservoir condition, the Reynolds number can be reformulated as a function of the total pressure, temperature and Mach number,

$$Re = \frac{p_0 L}{T_0^{n+0.5}} f(\gamma, M_\infty) C_1 \quad (31)$$

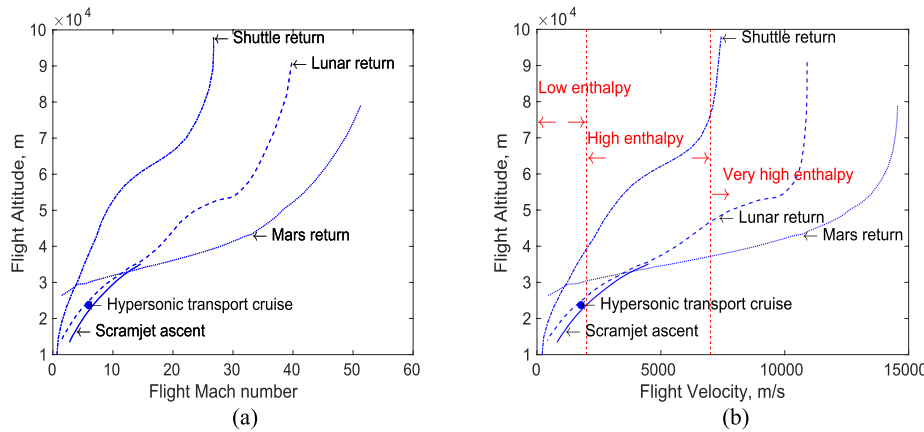


Fig. 17. Representative direct entry trajectories of typical flight vehicles [22,82–84] given in terms of the Mach number, (a), and velocity, (b).

where C_1 is a new constant. From the simulation requirement, $Re_{wt} = Re_{fl}$, then for identical Mach numbers it directly follows,

$$p_{0,wt} = \left(\frac{T_{0,wt}}{T_{0,fl}} \right)^{n+0.5} \frac{L_{fl}}{L_{wt}} \quad (32)$$

where L_{wt}/L_{fl} is the model scale. It is desirable to keep the wind tunnel total pressure and temperature as low as possible. The lower limit of the wind tunnel total temperature follows from the desired freestream Mach number and the condensation onset of air which is pressure dependent. However, typically the freestream temperature should not be lower than 50 K to avoid condensation. In this case the minimum total temperature amounts to 410 K for $M_\infty = 6$ and to 1050 K for $M_\infty = 10$. It is obvious that the wind tunnel total temperature can be less than the flight total temperature, for example the factor with the total temperature ratio in equation (32) is less than one resulting in a reduction of the wind tunnel total pressure. However, the wind tunnel total pressure is proportional to one over the model scale. This impressively shows the smaller the model scale the larger the necessary wind tunnel total pressure. In other words, large wind tunnel models allow lower reservoir pressures.

In case the freestream velocity should be replicated beside of the Mach and Reynolds number, for example in certain scramjet testing, it follows from the Mach number that the freestream static temperature and therewith also the viscosity are identical for both flight and wind tunnel. In this case the requirement of identical Reynolds number yields,

$$(\rho_\infty L)_{wt} = (\rho_\infty L)_{fl} \quad (33)$$

or for identical Mach numbers

$$\left(\frac{p_0}{T_0} L \right)_{wt} = \left(\frac{p_0}{T_0} L \right)_{fl} \quad (34)$$

Since Mach number and freestream static temperature are identical, the same holds for the total temperatures. Therefore, it follows,

$$\frac{p_{0,wt}}{p_{0,fl}} = \frac{L_{fl}}{L_{wt}} \quad (35)$$

which also results from equation (32) for $T_{0,wt} = T_{0,fl}$.

The dependence of the wind tunnel total pressure on the model scale leads to enormous total wind tunnel pressures for high Mach numbers. For example, Table 2 gives the necessary total pressure and temperature for a wind tunnel duplicating the flight Reynolds number for 35 km altitude as well as the flight Mach number and velocity for a typical model scale of 1:50 of a hypersonic transport vehicle. The data in Table 2 has been determined for equilibrium air chemistry. This simple example notably shows that for continuous running facilities there is not only a limitation due to power requirements but also due to the necessary high

Table 2

Necessary wind tunnel total pressure and temperature for duplicating flight Mach number, Reynolds number and flight velocity at 35 km altitude with a model scale of 1:50.

M_∞	4	5	6	7	8	9
$p_{0,wt}$, MPa	4.4	16.5	54.5	162	444.4	1140
T_0 , K	960	1325	1750	2220	2730	3280

total pressures and temperatures. For the continuous running facilities there is a clear Reynolds number limitation as shown for the AEDC tunnel B and C facility in Fig. 18. For impulsive facilities like blowdown facilities and gun tunnels, AEDC tunnel 9 yields the highest performance. But the limitation of the wind tunnel stagnation temperature (Tunnel 9, $T_{0,max} = 930$ K at $M_\infty = 8$) does not allow a simulation of the freestream velocity. Only tunnel C at $M_\infty = 4$ allows a simulation of the freestream velocity, but in this case the Reynolds number is limited to 23 million (not shown in Fig. 18).

The low enthalpy facilities mentioned in section 3.1, such as continuous, blowdown and gun tunnels, produce test conditions with low static temperatures of typically around 50–100 K. Consequently, as shown in Fig. 18, the Mach-Reynolds simulation capabilities of these facilities are not bad considering that the total pressures and total temperatures of these facilities are generally less than 100 MPa and 2000 K respectively, though the AEDC tunnel 9 could achieve total pressures of up to 150 MPa [26]. The reference length in Fig. 18 was chosen as twice the nozzle exit diameter, which is approximately the maximum allowable length of slender wind tunnel test models [29]. However, it is important to note that, because of their relatively low total temperatures they are restricted to so-called cold hypersonic flow phenomena. The limited total temperatures are due to technological limits of the continuously working heaters. Of course, the big advantage of these facilities is given by their long running time which allows detailed and accurate measurements of various flow and model parameters. Despite the limited total temperature and the necessity to avoid flow condensation, the Mach number capability of these facilities is still sufficient for duplicating the values of interest. Nevertheless, for hypersonic transport vehicles flying between 25 and about 30 km altitude and having typically 30–70 m length the Reynolds number is in the order of 100–300 million. This is well beyond the scope of most of the hypersonic facilities as shown in Fig. 18. Only tunnel 9 of AEDC might be able to generate these high Reynolds numbers with sufficiently large wind tunnel models. For these high Reynolds number tests, the boundary layer is turbulent. For low Reynolds number tests, tripping of the boundary layer is a usual technique. But at hypersonic Mach numbers, tripping is only efficient for Reynolds numbers which are not too low. The state of the boundary layer has strong influence on its separation

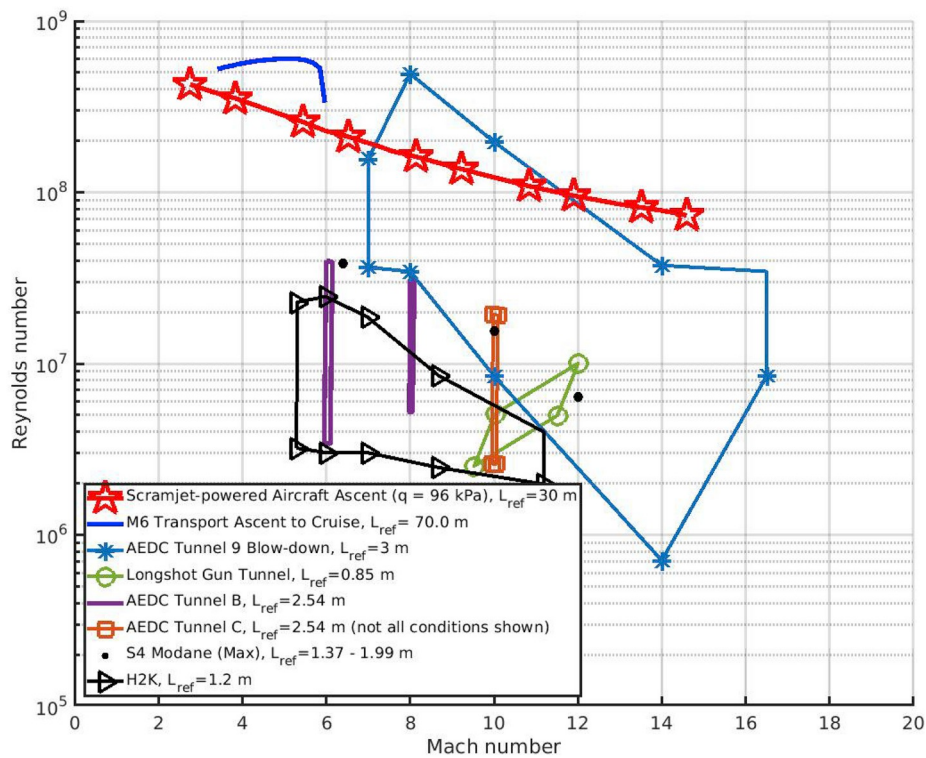


Fig. 18. Reynolds number versus Mach number capabilities of low enthalpy facilities compared to flight trajectories [25–27,29,85].

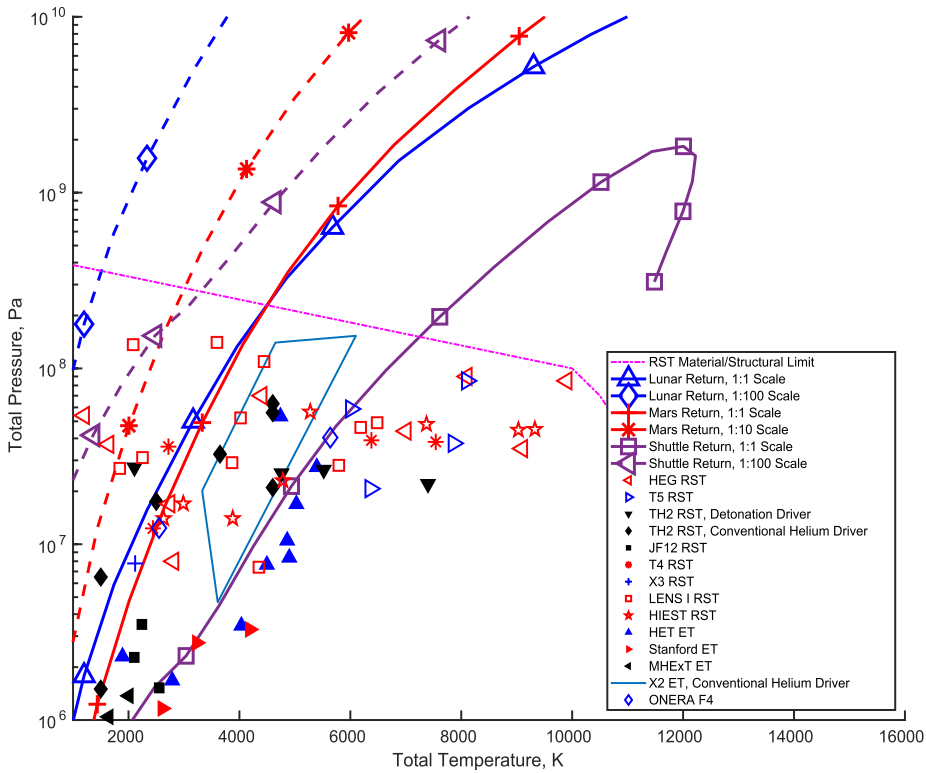


Fig. 19. Total pressure and temperature requirements under thermochemical equilibrium compared with high enthalpy facilities. RST and ET refer to reflected shock tunnels and expansion tunnels respectively [33,36,38,45–48,71,91–97].

behaviour, friction drag, shock boundary layer interactions etc. and is therefore of overall importance. A lack of Reynolds number capabilities therefore represents a severe limitation of aerodynamic wind tunnel testing.

4.1.2. High enthalpy regime

For the high enthalpy flow regime (see Fig. 1) the temperature behind strong shocks is sufficiently high to initiate chemical reactions. It was shown in chapter 2.1.2 for dissociation reactions the ρL -scaling law

holds. So, in addition to Mach and Reynolds number, the ρL -scaling should also be satisfied which also requires the duplication of the flight velocity. In this case, for matching the Reynolds number, the duplication of the freestream static temperature is necessary. The ρL -scaling directly shows that for downsized wind tunnel models the freestream density has to be higher than in flight. Since for the considered case the freestream static temperature should be the same as in flight, for the wind tunnel the freestream pressure and therewith the total pressure increases proportional to one over model scale. For perfect gas, this is particularly obvious from the corresponding equations for isentropic flow. However, for the high enthalpy flow regime the total temperature reaches high values and accordingly the required total pressures and temperatures for ground testing, shown in Fig. 19 calculated for equilibrium air, also reach high values. Total temperatures up to 10000 K can be achieved by reflected shock tunnels which are the most common type of facilities in the temperature range from about 1500 K to 10000 K. This figure already shows that for reasonably small models, a simultaneous duplication of ρL , U_∞ , Mach number and Reynolds number is only possible for a very small part of the trajectory. For the Shuttle return, with a feasible model scale of 1:100 only the LENS I facility and HEG are able to fulfil the requirement for the simultaneous duplications, but only for a low temperature range up to 2000 K. For the temperature range of interest, 3000 K–8000 K, there is no facility which fulfils this simulation requirement.

Limitations of today's existing metallic materials restrict reflected shock tunnels to total pressures of about 100 MPa at 10000 K total temperature. Consequently, only the lower end of the flight trajectories can be simulated with respect to simultaneous Mach number, Reynolds number, ρL and flight velocity duplications, even if a full scaled test model is used. Even smaller portions of flight trajectories can be tested if scaled test models have to be used, which is the case in most facilities. Nevertheless, in cases where flight conditions can be simulated by a reflected shock tunnel, good quality experimental measurements can be taken due to the typically longer test times and larger test models in reflected shock tunnel experiments compared to expansion tube experiments. However, in other cases where a better defined thermochemical

state of the experimental test condition is particularly important, the expansion tube would be the preferred facility as discussed in section 3.3. Hence, it can be observed in Fig. 19 that expansion tubes are designed for lower performance conditions in addition to the high performance conditions in Fig. 23, for certain applications. For example, Gu et al. [80] developed a conventional helium driver for the X2 expansion tube in order to study the thermochemical nonequilibrium and radiation of CO₂ at a freestream static pressure of around 300 Pa and a velocity of around 2.8–4 km/s, which were too low to achieve using the free piston driver. Laboratories fortunate enough to have both an expansion tube and a reflected shock tunnel, such as the Centre for Hypersonics at The University of Queensland with X2&3 [86] and T4 [62], the Graduate Aerospace Laboratories at California Institute of Technology with HET [48] and T5 [87], Calspan at the Buffalo Research Center with LENS XX [24] and LENS I & II [43], State Key Laboratory of High-Temperature Gas Dynamics at the Chinese Academy of Sciences with JF10&12 and JF16 [88], and JAXA with HEST [40] and HVET [89] as well as HEK-X [90], allow experimentalists to benefit from the advantages of both facilities and permits a comparison between the results to insure that findings are facility independent.

Duplication of the most important similitudes in high enthalpy flow - Mach number, Reynolds number, ρL and total enthalpy - is not easy to achieve. Still, although some phenomena require the recreation of all these similitudes, the study of some other types of hypersonic flows might suffice from the duplication of just some of the scaling parameters. In the case of a blunt body flow, real-gas effects would be the dominate phenomenon of interest and that means the simulation of ρL and the freestream velocity, U_∞ , is most important. Therefore, a ρL versus velocity graph shown in Fig. 20 is created to study the capabilities of the facilities in this aspect. For each facility, the reference length, L_{ref} , is defined as half of the core flow diameter, or 1/3 of the nozzle exit diameter for cases where the core flow size is unavailable. For the Mars and Lunar return capsule, the diameter of the FIRE II and Apollo 11 capsules respectively were used as L_{ref} . For the shuttle, its fuselage length of 33 m was used as L_{ref} . It has to be mentioned that due to the high total pressure requirements, shock tunnels usually are operated at

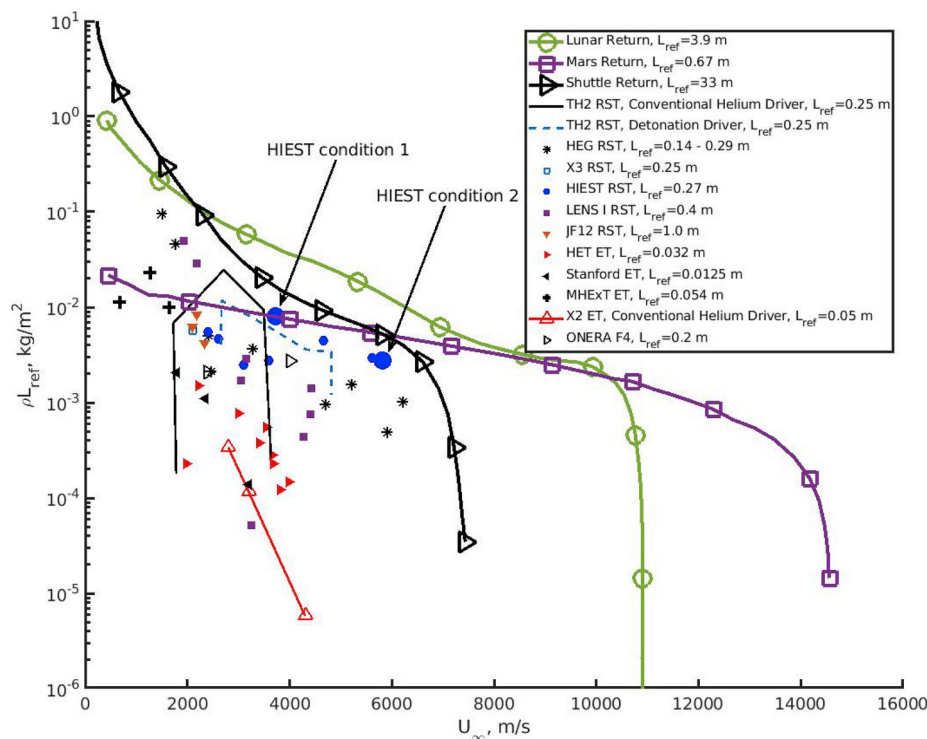


Fig. 20. ρL versus velocity capabilities of high enthalpy facilities compared to flight trajectories [33,36,45–48,71,91–95,98,99].

lower Mach numbers than the flight Mach number. In this case the freestream density is higher and consequently the ρL -scaling law can be satisfied for higher flow velocities. The lower Mach numbers are argued by the Mach number independence principle which holds for higher Mach numbers but strictly only for blunt bodies or strong shocks. Therefore, this strategy has to be carefully considered, for example, for slender bodies or for flows for which high-temperature gas effects as well as Mach and Reynolds number effects are important.

It can be observed that the facilities shown in Fig. 20 can simulate the real-gas effects on the Mars return and shuttle flight vehicles at velocities around 2–6 km/s but fails to simulate the high velocity part of the Lunar return trajectory. This is because, while the Mars return and Lunar return trajectories are similar, the Lunar return capsule, Apollo 11, is an order of magnitude larger than the Mars return capsule, FIRE II. This meant that a larger ρL requirement is necessary for Lunar return flight simulations. Nonetheless, manned missions to Mars have been proposed using spacecrafts with diameters of around 10–20 m [100], which are even larger than the spacecrafts used in manned missions to the Moon. Due to their size, the flow past these human-scaled configurations are difficult to simulate in wind tunnels. It is also important to note that many of the facilities shown in Fig. 20 were probably never designed to provide real gas simulation of Earth re-entry vehicles in the first place. For example, the conventionally driven X2 expansion tube was designed to study thermochemical nonequilibrium and radiation of CO₂ past a wedge model for Mars entry applications [80], while the JF12 reflected shock tunnel was designed to simulate slender hypersonic vehicles flying

at a speed of around Mach 7 and at an altitude of around 35 km [23].

Beside high-temperature real gas phenomena, Mach and Reynolds number effects are also of importance which should be simulated in the high enthalpy flow regime as well. Boundary layer growth, local heating rates, flow separation behaviour, shock boundary layer interactions are only a few of the phenomena which are strongly dependent on Mach and Reynolds number. Therefore, also for the high enthalpy flow regime the Mach – Reynolds performance of ground testing facilities is of interest. Fig. 21 shows the Reynolds number versus Mach number capabilities of various high enthalpy facilities mainly reflected shock tunnels and expansion tunnels compared to the different flight trajectories. The considered vehicles are of blunt body shape, therefore as reference length for the lunar and Mars return the typical vehicle diameter has been chosen and for the shuttle its body length because of its large angle of attack in this flight regime. For the wind tunnels as reference length the maximum feasible blunt body model diameter has been chosen which was estimated as half of the core flow diameter. From Fig. 21 it is obvious that only the LENS facilities, HEG, T6 and the HXT expansion tunnel are able to simulate a part of the lunar and Mars return trajectories up to Mach numbers of about 8–10. For this Mach number range, the Reynolds numbers for the Mars return trajectory are an order of magnitude lower caused by the shorter reference length which corresponds to the diameter of a typical Mars return sample probe. It is also obvious that the simulation range of the high enthalpy facilities is limited to a maximum Mach number of about 10. As mentioned above, this ensures high freestream densities and therewith positively

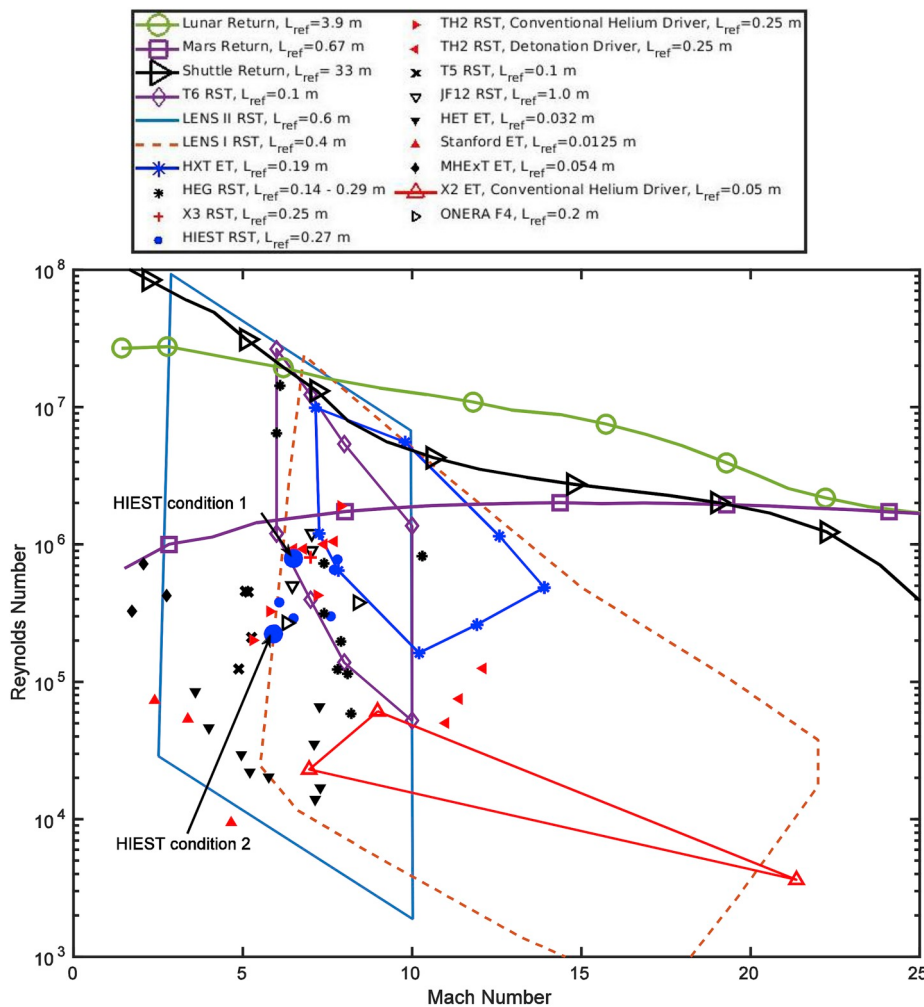


Fig. 21. Reynolds number versus Mach number capabilities of high enthalpy facilities compared to the blunt body re-entry trajectories [33,36,43,45–48,71,91–99, 101,102].

influences the ρL and Reynolds number simulation capabilities. However, there is a big discrepancy between the $\rho L - U$ simulation capabilities and the Mach – Reynolds number performance for high stagnation enthalpies. Comparing the ρL simulation capabilities in Fig. 20 with the Mach – Reynolds number performance in Fig. 21, the flow conditions yielding high ρL values at high velocities are achieved for a low Mach number, low Reynolds number flow condition. Since the Mach number is kept as low as possible to achieve a high density, this results in high freestream static temperatures reducing the Reynolds number. This is demonstrated exemplarily in Figs. 20 and 21 by the marked data points indicating the same flow conditions for two HEST conditions. The two conditions are close to the ρL trajectory for the Shuttle return, but they are far off from the trajectory concerning Mach and Reynolds number. This is the usual behaviour for high enthalpy testing.

For more slender configurations a reference length based on the body length is meaningful. For example, scramjet powered vehicles may fly as slender body configurations at low to medium total enthalpy conditions. As stated in section 2.2 the simulation of the flight velocity or the corresponding total enthalpy in ground testing in addition to the ρL -scaling is important for a correct simulation of the combustion processes. Because of the additional importance of Mach-Reynolds number effects for this type of vehicles, Fig. 22 shows the Mach-Reynolds simulation capabilities of the corresponding wind tunnel facilities compared to a scramjet-powered ascent flight trajectory of a vehicle of 30 m length. For the ground test facilities, the reference length was chosen as twice the nozzle exit diameter, which approximately represents the maximum length of a slender body wind tunnel model [29]. Only T6, the LENS facilities and HEG come close to the flight trajectory for a narrow Mach

number regime at about five to seven.

4.1.3. Very high enthalpy regime

Fig. 23 shows the total pressure and temperature requirements to simulate the ρL -scaling, Mach number and Reynolds number for blunt body return trajectories compared to the simulation range of some expansion tunnels. Unfortunately, no total pressure and temperature data was available for the LENS XX facility in literature. Therefore, in this chart the performances of this facility are missing. It is clear from the figure that using scaled test models significantly increases the total pressure requirements of the ground test facilities. Thus, obtaining sufficiently high total pressure conditions may be the most difficult challenge for ground test facilities. While reflected shock tunnels struggle to achieve total pressures of more than 10^8 Pa, expansion tunnels can achieve total pressures of more than 10^{10} Pa which is not particularly surprising given the huge total pressure gains across an unsteady expansion as shown in Fig. 15. For example, Gildfind et al. [22] operated the free piston driven X2 expansion tube with a secondary driver to produce medium enthalpy conditions with total pressures around 10^9 – 10^{10} Pa for the purposes of scramjet testing. These conditions allow for the testing of scramjets as small as 1/10 of flight. Fig. 23 shows that these same conditions can also be used to simulate the medium enthalpy portions of the shuttle, lunar return and Mars return flight trajectories for certain model scales. Similar conditions could have been generated by the free piston driven RHYFL expansion tube [103] and the free piston driven HYPULSE expansion tube [104], but these facilities were just designed and never completed.

Note that for Lunar return and Mars return, a large portion of the

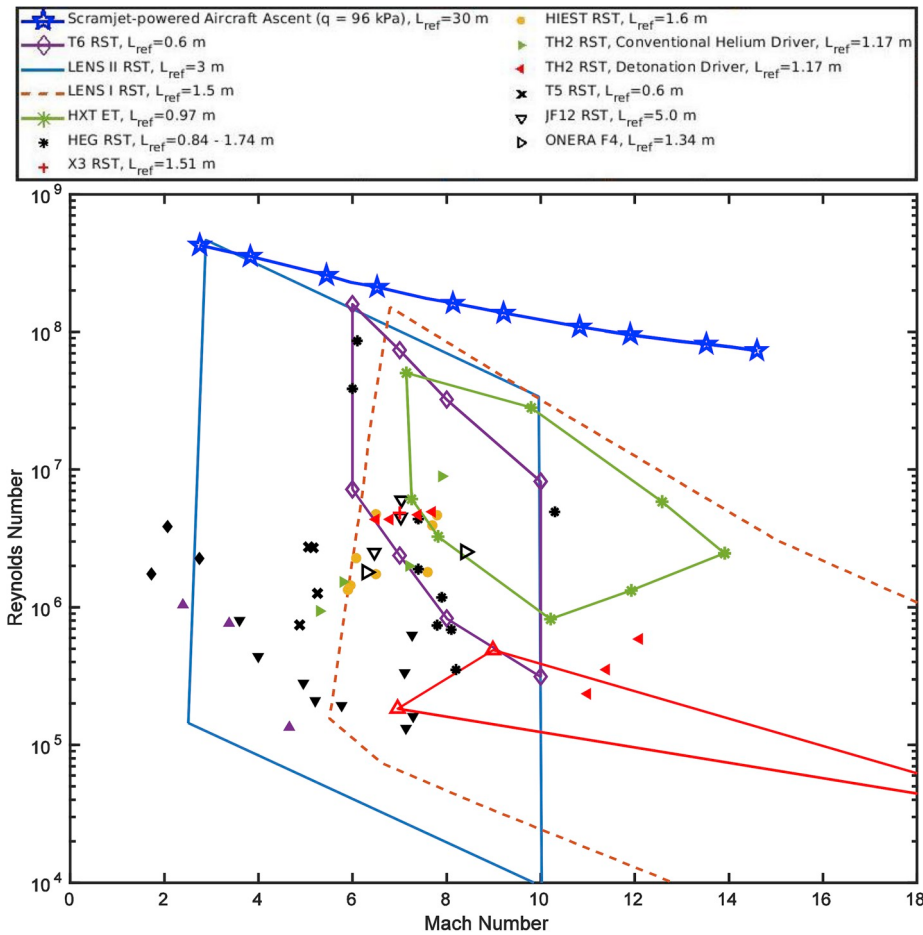


Fig. 22. Reynolds number versus Mach number capabilities of high enthalpy facilities compared to the scramjet flight trajectory [33,36,43,45–48,71,91–99, 101,102].

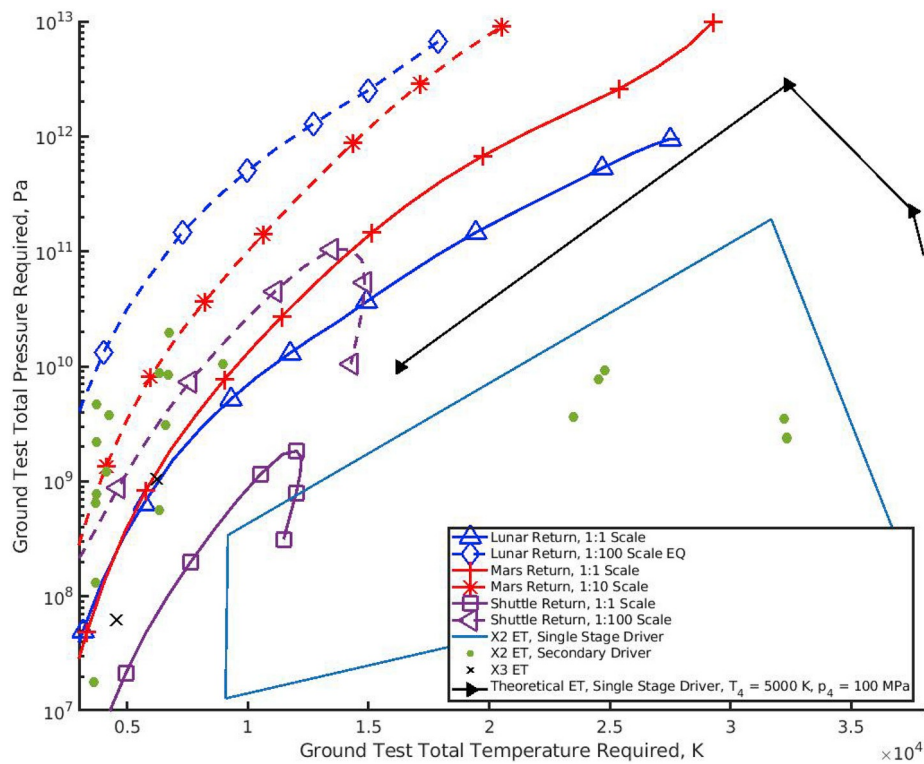


Fig. 23. Total pressure and temperature requirements under thermochemical equilibrium compared with the performance of expansion tunnels [22,49–51].

trajectory is in the high enthalpy region where the total temperature is greater than 15000 K. In such cases, as shown in Fig. 23, neither the existing expansion tubes nor the conceptual expansion tubes could provide high enough total pressures, even if full sized test models are used. This is because the particular drivers of the expansion tubes were not designed to facilitate these conditions. For example, the free piston driver of the X2 expansion tube, which can heat helium up to 3000 K [105] to achieve a speed of sound ratio, a_4/a_1 , of 9.4 for air as the test gas, is not particularly powerful for a free piston driver and it was never designed to provide total pressures of more than 10^{11} Pa at total temperatures of more than 15000 K [64]. Consequently, this issue may be resolved by providing expansion tubes with higher performance free piston drivers to specifically support flight simulation of these high enthalpy conditions [106]. For estimation of the maximum performance of an expansion tunnel operating with a helium piston driver, a maximum driver pressure of 100 MPa and a driver gas temperature of 5000 K has been assumed. From the currently available technology this seems to well represent the maximum achievable conditions. Even higher pressures and/or temperatures would cause burning of piston seals, strong erosion and other problems. Helium is assumed as driver gas because of its high performance and its ease of handling without any safety precautions. Hydrogen as driver gas would significantly increase the tunnel performance but at the expense of having highly demanding operations and extensive safety precautions. From the PITOT code [55], the approximate theoretical upper limit of performance for this fictitious expansion tunnel operating without a secondary driver is shown in Fig. 23 for realistic fill conditions in the shock and acceleration tube, and assuming thermochemical equilibrium throughout. Compared to X2 operating with a single stage driver, the maximum total temperature increased by about 5000 K, while the maximum total pressure increased by approximately an order of magnitude. Although this fictitious expansion tunnel comes close to duplicating the total temperature and pressure required for simulation of a full scale lunar return vehicle at the very high total temperature region, there is more to be desired in terms of simulating the Mars return and scaled lunar return conditions. Stalker

mentioned that there are no theoretical performance limitations of a free piston driver [1]. Though, practical limitations may include heating the driver to temperatures so high that the facility wall begins to melt, significant heat loss due to radiation and containment of the high pressure driver gas. Furthermore, there is the known Page-Stalker loss mechanism for free piston drivers [87].

The ρL -scaling capability of the expansion tunnels is shown in Fig. 24. From this figure, the LENS XX expansion tunnel [24] seems to be capable of almost complete ρL simulation of all the trajectories of flight vehicles considered. The X2 expansion tunnel is capable of ρL simulations at velocities of around 3–4 km/s but falls slightly short at higher velocity conditions. The T6 expansion tunnel [101], which is currently being developed, looks to have similar ρL capabilities as the X2 expansion tunnel. The reason why the LENS XX has distinctly better ρL capabilities compared to the other expansion tunnels is due to its size. The LENS XX theoretically allows for the use of a 0.8 m diameter test model which is significantly larger than that allowed in the second biggest expansion tunnel, the X3 expansion tunnel, of 0.24 m [50]. The LENS XX actually has similar ρ versus velocity capabilities as the X2 expansion tunnel, but because LENS XX is much bigger than X2, the ρL capabilities of LENS XX is superior to that of X2. Concerning this data, it is very important to note the following: as reference length in Fig. 24, half of the core flow diameter has been taken which is the usual procedure described in literature.

At the highest enthalpy conditions, all shown expansion tunnels have a useful running time of about 100–200 μ s. Considering the slug of accelerator gas upstream of the test gas has approximately a flow time of one third of that of the test gas, which is a good rule of thumb [46], the total time available for flow establishment of the test model is about 130–270 μ s. If a sufficiently long steady state flow time is required, then the flow establishment time puts a severe limitation on the maximum allowable model size, which is discussed in detail in section 4.2.1. From this follows (see Table 3) that if 270 μ s is available for flow establishment at a flow velocity of 10 km/s, then the maximum allowable model size is only 30 mm for separated flows and 90 mm for attached flows. For

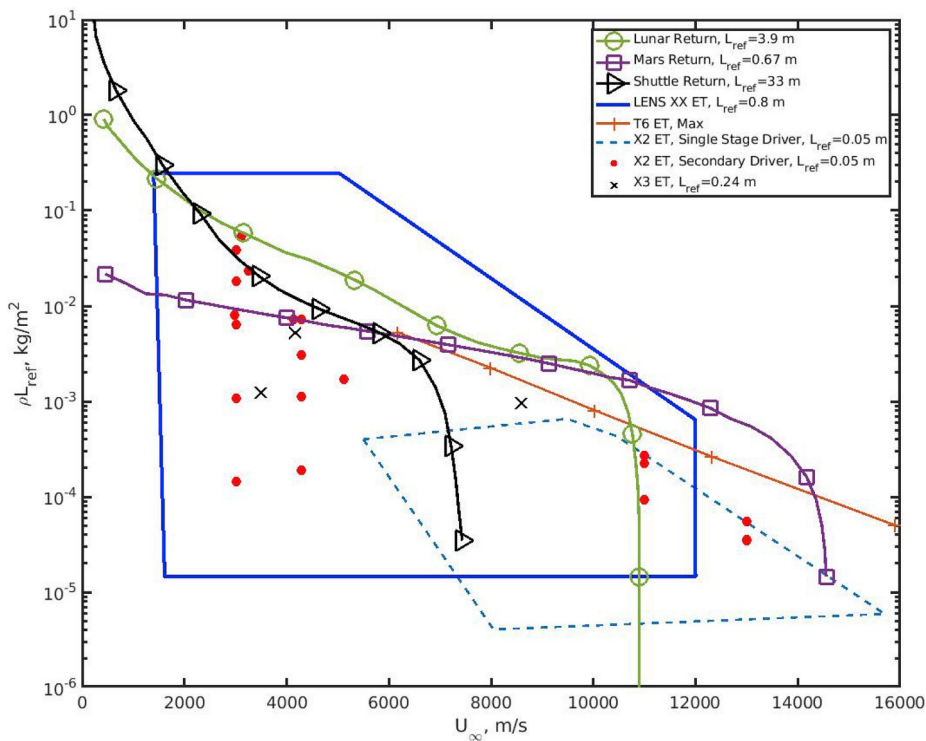


Figure 24. ρL versus velocity capabilities of expansion tunnels compared to the flight trajectories. L_{ref} values are based on half the core flow size, not on allowable model size for flow establishment [22,24,49–51,101].

Table 3

Maximum model size for attached ($K = 10$) and separated ($K = 30$) flows which ensure a flow establishment time, t_e , of 33% of the running time after flow initiation. The notations t_m and L_e represent the wind tunnel test time and the characteristic length of the test model respectively.

U_∞ , m/s	2000	4000	6000	8000	10000
t_m , ms	6	3	1.5	0.4	0.27
t_e , ms	2	1	0.5	0.13	0.09
L_e , m ($K = 10$)	0.4	0.4	0.3	0.11	0.09
L_e , m ($K = 30$)	0.13	0.13	0.1	0.036	0.03

these model sizes, the ρL values for the LENS XX facility would subsequently reduce by an order of magnitude. The model size constraint would also cause the ρL capability of X3 to be appreciably reduced. For T6, no reference length has been given, only the product ρL . This analysis impressively shows that the available testing time poses a severe limitation on the allowable model size and therewith on the ρL simulation capability of expansion tunnels. Additionally, it should be mentioned that a model size of tens of millimetres does not allow for much instrumentation on the model.

It is important to note that a category of flight trajectory not shown in Fig. 24 is that of meteoroid entries. Meteoroid entries occur at velocities of around 25–30 km/s on average [107]. Hence, none of the expansion tunnels shown in Fig. 24 comes close to duplicating these velocities. Research in meteoroid entry is now gaining prominence [107,108]. Consequently, in the future, there would likely be motivation to install more powerful drivers in expansion tunnels to facilitate the study of meteoroid entry, which would also simultaneously allow for even greater ρL capabilities. Nevertheless, it is important to note that, while theoretically the velocity attainable in the expansion tube can increase to very high values with increase in driver performance, the static temperature of the test flow may eventually be so high that the thermochemical state of the test flow resembles nothing like flight. This may be an effective velocity limitation of expansion tubes in terms of

simulating flight.

The Mach-Reynolds number performance of expansion tunnels is shown in Fig. 25 and compared with blunt body re-entry trajectories. The LENS XX and X2 with secondary driver allow a simulation of the blunt body trajectories over a wide range of Mach numbers. However, as for the high enthalpy facilities, it has to be kept in mind that the points in the ρL and the Mach - Reynolds number chart do not correspond to each other. Probably even more important is the fact that as mentioned above, the chosen reference length is that typically used in literature. But as before, the resulting model size does not allow a full flow establishment during the running time. For sufficiently small models of about 23 mm for blunt bodies according to Table 3, the Reynolds number drops significantly and there is no longer a match with the flight trajectories.

The Mach-Reynolds number performance of expansion tunnels compared with a scramjet ascent trajectory is shown in Fig. 26. Apart from the X3 expansion tunnel and the X2 expansion tunnel operated in single stage driver mode, the expansion tunnels in Fig. 26 come close to providing Mach-Reynolds simulations of the full-size scramjet-powered hypersonic aircraft. However, the reference length used is defined as twice the nozzle exit diameter. Hence, as mentioned in the preceding paragraph, due to the model size requirement for flow establishment, this probably results in a significant over estimate of the Mach-Reynolds number capabilities.

4.2. Other limitations

Aside from the performance aspects, reflected shock tunnels and expansion tubes in particular suffer from other limitations. These other limitations are related to the test time, test model size and the flow quality. This section will focus on these topics.

4.2.1. Test time and model size

Although the test time of reflected shock tunnels are considered long relative to the high enthalpy facilities discussed in section 3.3, it could

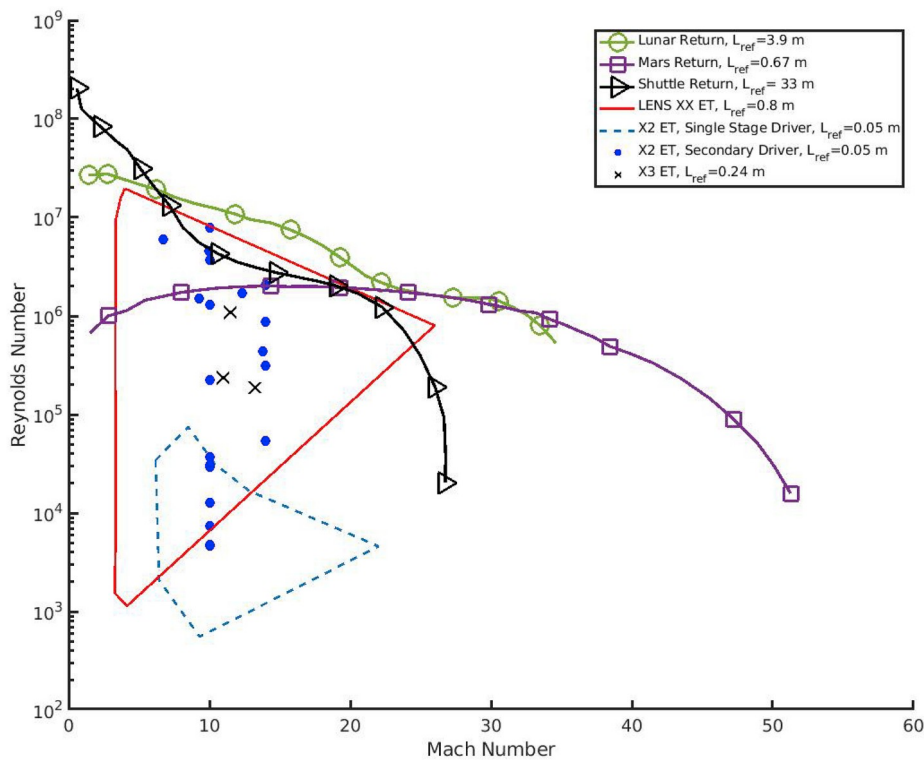


Fig. 25. Reynolds number versus Mach number capabilities of expansion tunnels compared to the blunt body flight trajectories [22,24,49–51].

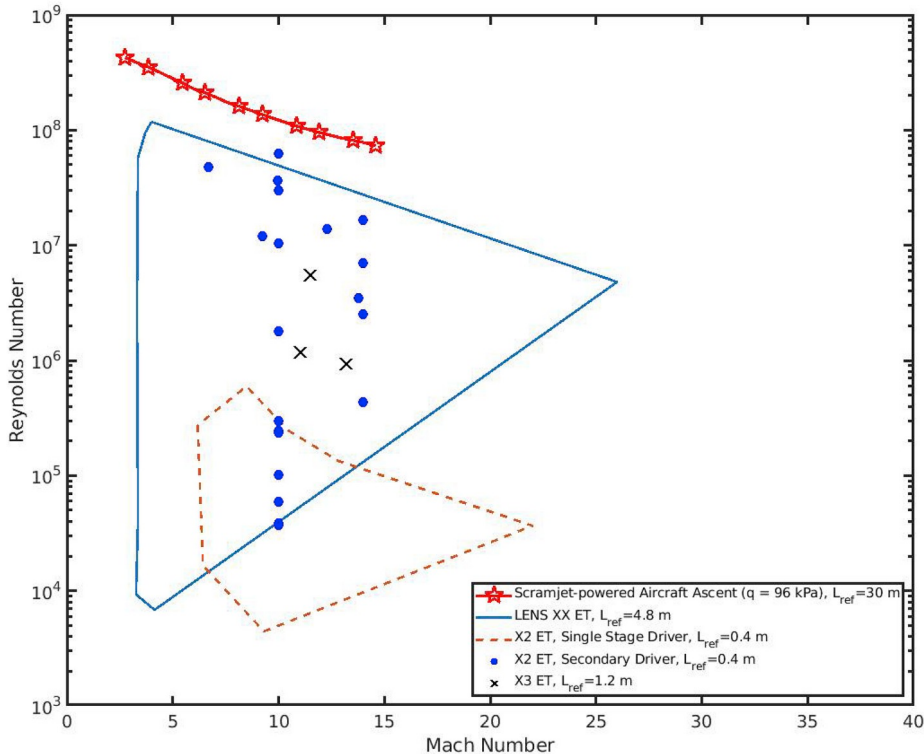


Fig. 26. Reynolds number versus Mach number capabilities of expansion tunnels compared to the scramjet flight trajectory [22,24,49–51].

be even longer under ideal conditions. Under inviscid conditions, the test time in reflected shock tunnels could end when the driver gas contact surface arrives at the test section. However, in reality, interactions between the reflected shock, contact surface and the boundary layer creates a wall jet of driver gas and vortices behind the reflected shock.

The vortices interact with the jet of driver gas, carrying it towards the centre of the shock tube and into the nozzle resulting in premature driver gas contamination [73]. This process is illustrated in Fig. 27 without the vortices. Other transport mechanism as vortical structures behind the reflected shock also lead to a premature driver gas

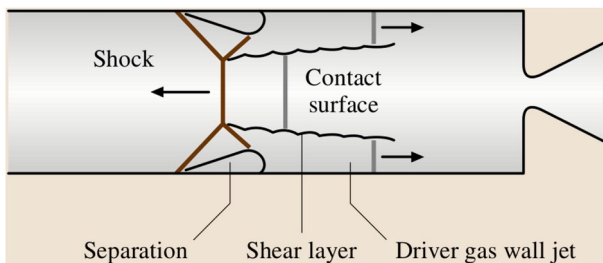


Fig. 27. Schematic of the reflected shock/boundary layer interaction which results in driver gas wall jets [58].

contamination. Consequently, significant work has been done to understand the general characteristics of this phenomenon and provide methods to experimentally detect the premature arrival of the driver gas at the test section.

An important characteristic of the shock/boundary layer interaction in Fig. 27 is that the severity of the interactions is essentially independent of total pressure but increases with increase in total enthalpy resulting in more significant driver gas wall jets, for a given facility [37, 65]. This is illustrated in Fig. 28 by Boyce et al. [37] for the T4 reflected shock tunnel. Part of the uncontaminated test flow will be wasted to start up the nozzle flow resulting in very little useful test flow at higher enthalpies. Eventually, the facility will produce test conditions with inadequate test times as total enthalpy increases. Consequently, the performance of reflected shock tunnels may often be limited by premature driver gas contamination rather than the more obvious material limitations. For the T3, T4 and T5 reflected shock tunnels, the total enthalpy is limited to about 25 [61], 15 [21] and 22 [65] MJ/kg respectively due to premature driver gas contamination. Stalker et al. [21] notes that the reason why T4 is particularly susceptible to premature driver gas contamination might be because its shock tube has a length to internal diameter ratio of 133 instead of the usual value of 80–100 and this extra length may have allowed extra turbulent mixing at the driver-test gas interface. From analysis of numerous contamination-free test time data from various facilities, Stalker postulated that the contamination free flow length increases with increasing shock tube diameter [1]. This makes sense because, as stated by Hornung [65], the relative importance of wall effects decreases with increase in diameter. A consequence of this is that a direct scale-up of a particular reflected shock tunnel would result in a relative increase in the total enthalpy limit from premature driver gas contamination. Alternatively, direct scaling of the shock tube and driver, while the nozzle size is kept the same, would result in larger increases in the test

time and subsequent larger increases in the total enthalpy limit. Though, eventually, the performance of the facility will be limited by the nozzle melt limit, which is discussed in detail in section 4.2.2, due to test times which are too long.

Due to the occurrence of premature driver gas contamination, various methods and devices have been made to experimentally measure the arrival of the driver gas in a reflected shock tunnel. One of the earliest methods to measure driver gas contamination was using a mass spectrometer to directly detect helium as demonstrated by Crane and Stalker in 1977 in T3 [111]. Another early method of detecting driver gas contamination was taking static pressure measurements at the nozzle exit as reported by Stalker and Morgan in 1988 for T4 [112]. An example of their measurement is shown in Fig. 29. It was taken using a flat plat with a pressure orifice located 200 mm from the leading edge which was located at the nozzle exit plane. Stalker and Morgan noted that, while the static pressure dropped distinctly after about 1.1 ms as shown in Fig. 29, the pitot pressure measurements remained roughly the same which likely indicates helium contamination due to the increase in heat capacity ratio caused by helium addition. Alternatively, Hornung in 1991 took high speed photography of the shock from a wedge, which was used to provide an indication of freestream helium content as the shock angle was also shown to be sensitive to helium presence in the freestream [87]. Subsequently, in 1996, Paull developed a device which works by choking of a small duct as the contamination rises above a preset level [109]. Also in 1996, like Stalker and Morgan in 1988, Kindl et al. measured the nozzle exit static pressure to determine helium contamination [113], except Kindl et al. used a small static pressure probe, shown in Fig. 30, instead of a flat plat as used by Stalker and Morgan. Various ideas like suction slots and a sleeve as insert at the end wall have been proposed to delay the helium contamination [72, 114, 115]. The sleeve in particular shows a positive effect for overtailored conditions. But the longest test times are still achieved without any device for slightly undertailored conditions [72].

In detonation driven facilities, whether the mechanism of driver gas contamination is the same as that of helium driver gas is uncertain. The experimental results of Olivier [35] indicated that the detonation driver gas contamination mechanism is qualitatively the same as that of helium drivers. However, the CFD investigation by Chue et al. [116] showed the opposite result where the detonation driver contamination mechanism was observed to be qualitatively the same but quantitatively more prominent compared to those for helium drivers, resulting in more severe driver gas contamination in detonation driven facilities. Most of the above methods for determining driver gas contamination are useless in situations where detonation drivers are used. At the test section, the detonation driver gas consists mainly of gaseous water which has a

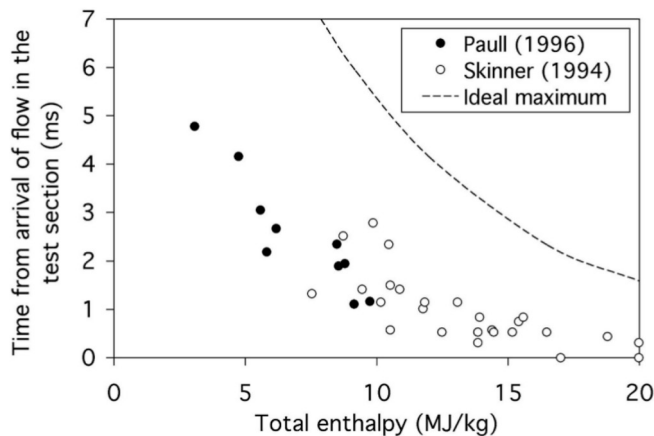


Fig. 28. The time of arrival of 7.5%, Paull (1996) [109], and 10%, Skinner (1994) [110], mole fraction of driver gas compared to the latest arrival of driver gas in an ideal case [37].

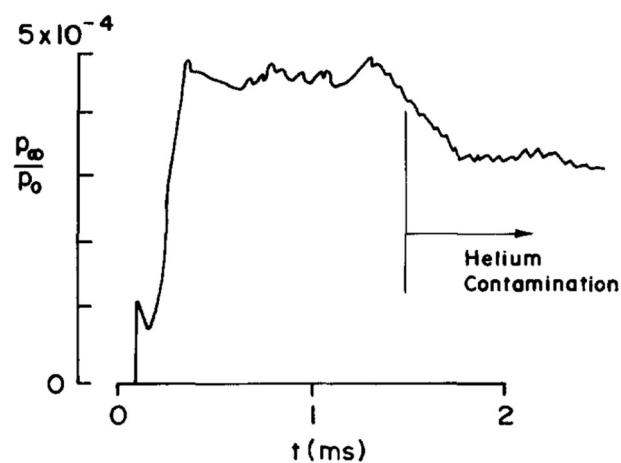


Fig. 29. Static pressure measurements in T4 at the test section using a flat plate [112].

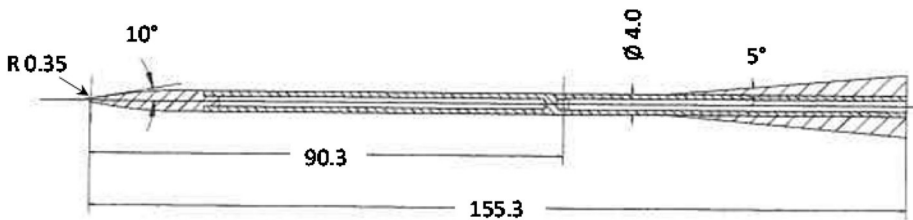


Fig. 30. Static pressure probe with dimensions in mm [113].

similar heat capacity ratio as the most commonly used test gas - air. Therefore, it is necessary to employ optical diagnostics for detecting driver gas contamination in detonation driven facilities [117], which are more complicated techniques compared to those used to detect helium driver gas.

While driver gas contamination determines the upper end of the test time, the necessary flow establishment time represents the lower end of the useful test time interval. In literature there are a lot of empirical and semi-empirical relations to estimate the flow establishment time, but there is no conclusive and reliable theory for this. This is not surprising because the flow establishment time depends on the model geometry, the type of establishment time determining flow phenomenon etc., in addition to the freestream conditions. In case of facilities utilizing the expansion of the flow in a nozzle, the nozzle starting process and the model flow establishment may happen in parallel, which complicates the estimation of the pure flow establishment time.

While the problem of helium wall jetting should not occur in expansion tubes [77,117], expansion tubes have inherently less test time than reflected shock tunnels, by an order of magnitude in general. Expansion tube test times are generally ended by the arrival of wave processes at the test section. There are generally three ways for the test time in an expansion tube to end. From Fig. 14, test time can be terminated by either 1) the tail of the secondary unsteady expansion fan, 2) the reflected head of the secondary unsteady expansion fan, or 3) the reflected head of the primary unsteady expansion fan, whichever occurs first. Which one of the three wave processes terminates the test time depends on the test condition and the facility dimensions, though most of the time it is either case 1 or case 2 because the driver section should be sized correctly so as to not interfere with the test flow. Paull et al. also postulated the possibility of a fourth way for test time termination where “bubbles” of driver gas, created due to mixing at the contact surface, get accelerated through the unsteady expansion and arrive at the test section prior to the wave processes [118].

Different flow phenomena take different amounts of time to establish. In general, inviscid flow phenomena need a much shorter establishment time than viscous ones. Steady flows establish much faster than pseudo-steady flows like some shock oscillation modes, etc. The flow establishment time, t_e , can be estimated by

$$t_e \approx K \frac{L_c}{U_\infty} \quad (36)$$

where K is a constant with a value depending on the flow phenomenon, L_c is the characteristic length and U_∞ is the freestream velocity. No exact data or theory exist which can accurately determine the flow establishment time or the value K in equation (36). As a rule of thumb, for attached flows the value of K should be about 3–10, and for separated flows at least 30 [46]. From this, in Table 3, the maximum possible model size has been determined from equation (36) as function of the flow velocity and typical flow establishment times, t_e . These have been assumed as one third of the typical measuring time, t_m , allowing for a sufficiently long quasi-steady flow period of two third of the overall measuring time. The values of t_m in Table 3 depend on the flow velocity and are representative of the corresponding facilities, i.e. conventional shock tunnels to 4000 m/s, piston driven shock tunnels up to 6000 m/s

and expansion tunnels from 8000 to 10000 m/s. The results show that especially for the high velocity range from 8000 m/s and higher, the short measuring times at these conditions require very small models which, beside the already mentioned reductions in the Reynolds and p-L simulation capabilities, would also not allow an extensive instrumentation. The only way to increase the amount of test time left over after flow establishment is to increase the facility size (tube length and diameter) while keeping the model size roughly constant or decrease the model size while facility size is constant. Hence, test time is one of the fundamental limitations of expansion tubes, and of reflected shock tunnels at high enthalpy conditions.

4.2.2. Limitation due to throat melting

Flow establishment time and remaining testing time are a severe concern mainly for expansion tunnels, while reflected shock tunnels must pay a performance penalty due to the throat-melt limit. As the test time is increased in the reflected shock tunnels, the throat of the nozzle will eventually experience surface melting. Significant throat melting during the experiment is highly undesirable because the throat diameter would increase causing changes to the test flow properties. Additionally, the melted products of the nozzle throat will form as contaminates at the test section and the melted throat surface may cause flow disturbances in the test section which is unwanted. Therefore, it is necessary to avoid throat melting. This means that as a reflected shock tunnel is scaled up, eventually, the total pressure and total temperature attainable in the facility will be limited by the throat melting while the strength of the facility structure becomes irrelevant.

Using Bartz's nozzle heating equation [119], the nozzle throat surface temperature was calculated for different total pressures and total temperatures at different throat diameters and at a constant nozzle throat diameter to nozzle throat radius of curvature ratio of 2. The results are shown in Fig. 31 for different nozzle throat materials. From the results, tungsten seems to be a good material based on the melting point, being able to withstand a total pressure and total temperature of 100 MPa and 7600 K respectively for about 10 ms. However, tungsten oxidizes strongly and this is responsible for direct removal of the throat material [87]. Hence, tungsten is not a good material for the nozzle throat. Steel, while it is good structurally, is particularly bad at withstanding transient heating as it melts after around 1 ms from a total pressure and total temperature of 30 MPa and 7600 K respectively, while copper is too soft for the high pressures of the nozzle reservoir region. Therefore, molybdenum seems to be one of the best materials, being able to withstand a total pressure and total temperature of 100 MPa and 7600 K respectively for more than 3 ms. For a reservoir state of 300 MPa and 10000 K, no material can allow for any reasonable amount of test time, while for a reservoir state of 9.7 MPa and 4250 K, the throat melt limit is irrelevant as even steel can allow for test times of more than 10 ms. Promising throat materials are tungsten-molybdenum alloys which combine the advantages of both materials. In industry these alloys are used for high thermally and mechanically loaded parts.

The nozzle throat heating mainly depends on total pressure and total temperature. There is a small dependence on the throat diameter, and an even smaller dependence on the throat diameter to throat radius of curvature ratio, hence this was kept constant at a value of two in Fig. 31. It can be seen in Fig. 31 that, given a certain test time, there is a limit for

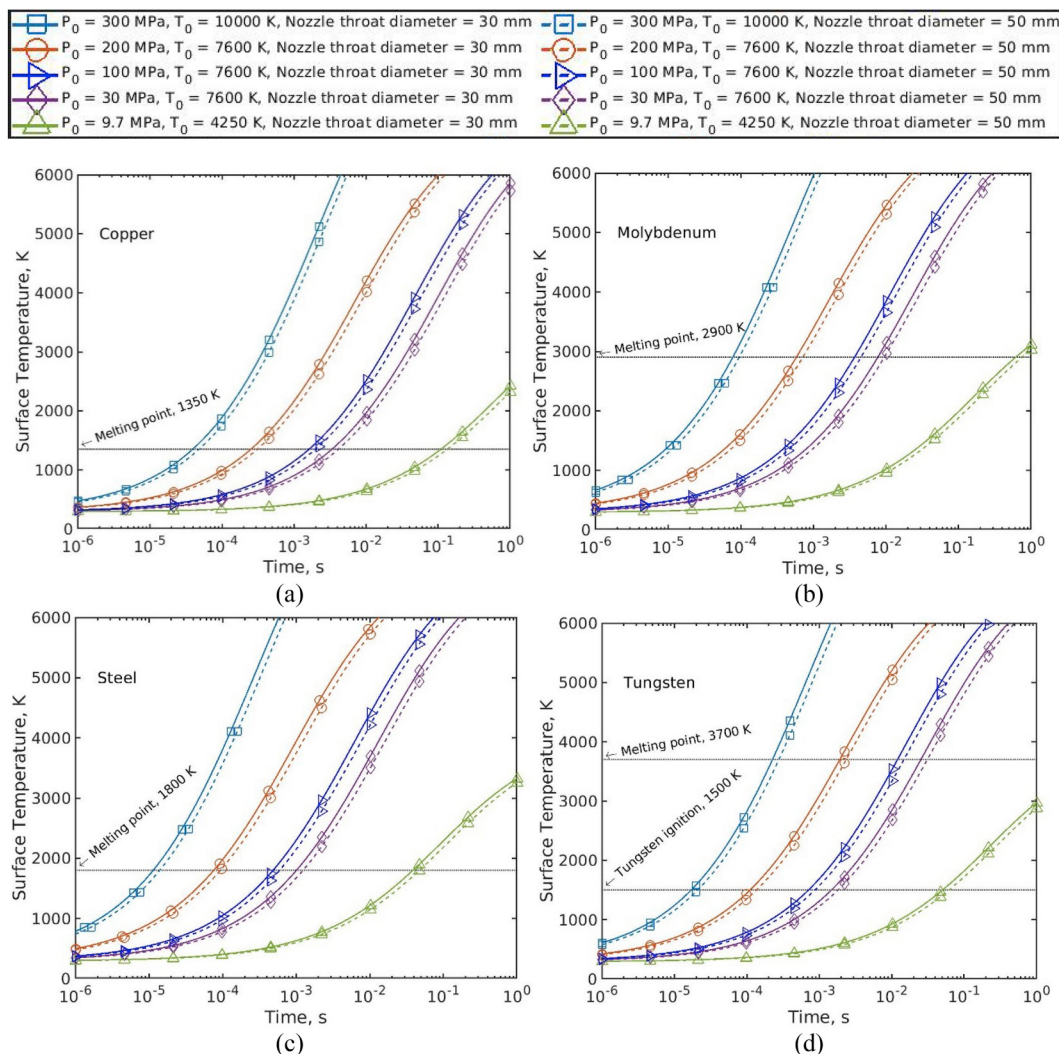


Fig. 31. The nozzle throat surface temperature versus time of different materials for different total pressures and total temperatures at different throat diameters and at a constant nozzle throat diameter to nozzle throat radius of curvature ratio of 2.

the nozzle reservoir condition in order to avoid throat melting. For example, if the facility has a test time of 10 ms and a nozzle throat made out of molybdenum, the nozzle reservoir condition must be less than about 30 MPa and 7600 K in order to avoid throat melting. Hence, large reflected shock tunnels with long test times generally cannot produce high performance conditions. Therefore, the only way to produce high performance conditions in large facilities is by shortening the shock tube so that the test time is compressed. Nevertheless, there still needs to be enough test gas to establish a steady flow in the nozzle and around the test model. A significant portion of the available test time in Fig. 31 is wasted on nozzle start-up. So there could be situations where the throat melts before a steady flow can be established.

4.2.3. Measurement techniques

Limitations not only exist concerning wind tunnel performances, but also concerning applicable measuring techniques. As for the simulation performances, the applicable measuring techniques can be assigned to the different types of wind tunnels or the different flow regimes characterized in this paper by low, high and very high enthalpy regimes.

For the continuous running and blowdown facilities nearly all measuring techniques known from subsonic and supersonic flows are applicable. For low stagnation temperatures up to 1000 K even hot wire anemometry is possible. For higher stagnation temperatures focusing laser differential interferometry has been successfully applied. For these

facilities this also allows the measurement of freestream turbulence levels which is an important parameter for characterizing the boundary layer transition behaviour in hypersonic flows. These facilities also allow accurate aerodynamic force and moment measurements due to their long running times. Heat transfer measurements are performed on a more or less routine basis but here the long running time is of disadvantage because lateral heat conduction effects influence the measured heat transfer normal to the wall. Other measuring techniques are also applied which are listed in Table 4.

Several attempts have been made to measure freestream turbulence levels in shock tunnels. But till today no reliable measurement has been performed. Also force and moment measurements are difficult to perform. Fast force balances have been developed which in conjunction with acceleration compensation techniques allow force and moment measurements for measuring times down to 2 ms. A few years ago a free-flight force measurement technique has been proposed and successfully tested in the HIEST facility which might be promising for short-time force and moment measurements, and also for complicated model geometries [120].

The measuring time in the range of milliseconds make shock tunnels well suited for heat flux measurements because it is long enough to ensure a full flow establishment and short enough to reduce the effect of lateral heat conduction to a very low level. In expansion tunnels attempts have been made for measuring aerodynamic forces by stress bars.

Table 4

Standard measuring techniques of different types of test facilities.

Facility	Continuous and blowdown facilities	Shock tunnels	Expansion tunnels
Type of measurements	Total temperature	–	–
	Total pressure	Total pressure	–
	Freestream temperature	(Laser methods)	–
	Freestream pressure	Freestream pressure	–
	Freestream velocity	(Laser methods)	–
	Freestream turbulence level	–	–
	Model surface pressures, local and surface mapping	Model surface pressures, mapping	Model surface pressures, local
	Model surface temperature and heat fluxes, local and surface mapping	Model surface heat fluxes, mapping, line scan, infrared thermography	Model surface heat fluxes, local
	Surface shear stresses	–	–
	Flow velocities, local and 2d	–	–
	Overall forces and moments	Overall forces and moments	(Stress bars)
	Forces and moments of flaps, rudders etc.	–	–
	Oil flow visualization	–	–
	Flow visualization	Flow visualization	Flow visualization

However, this is an even more complex technique which is far from regular use, and there is still the question of flow establishment and remaining testing time. A further problem of high enthalpy testing which, amongst others, pose a severe limitation for laser based measuring techniques is the pollution produced in the facility which results from bursting diaphragms, sealing of pistons etc. and the erosion of the tube and inner nozzle surface at highly loaded locations. The pollutants form a layer at the inner tube surface and part of it is transported by the test gas flow to the test section and model surface during the experiment. This facility dependent pollution increases with increasing total enthalpy. To the author's knowledge there is no facility avoiding this problem of dust and particle pollution. There are several attempts for performing non-intrusive laser based measurements e.g. of the species concentration at the nozzle exit flow for reflected shock tunnels. But the problem mentioned above and others still lead to a high uncertainty for these measurements.

5. Conclusion

In this paper, the methodologies of hypersonic ground testing were reviewed. Then the characteristics and capabilities of the different hypersonic wind tunnels were discussed. The capabilities and limitations of these facilities were quantitatively assessed in regards to the simulation of relevant flight vehicles. In addition, other limitations of the ground test facilities, such as test time, test model size and applicable measuring techniques were assessed for the most important facility types for modern hypersonics research.

The facilities were grouped into three categories according to three typical flow regimes characterized by low, high and very high total enthalpies or flow velocities. Each category of facility has its own advantages and disadvantages concerning performances, flow quality, measuring time etc. Low enthalpy facilities like continuous running and blowdown facilities allow the longest running times, detailed measurements and best knowledge of freestream properties, but are limited to low stagnation enthalpies and therefore exclude the regime of reacting hypersonic flows. From the listed facilities only the AEDC Tunnel 9 is capable of a full Mach-Reynolds number simulation of most of the flight trajectory of a Mach 6 hypersonic vehicle with typically 30 m length. Problems become more severe for the high enthalpy flow regime. Conventional, detonation driven and free-piston driven shock tunnels are the most popular facilities operated at these conditions. The short running times pose a challenge for force and moment measurements and other measuring techniques. Additionally, a full Mach-Reynolds number simulation is not possible for these flow conditions because of the required huge stagnation pressures. These also limit the facility performance because of the direct dependence of facility integrity and nozzle throat melting issues on the stagnation conditions. Expansion tunnels

allow much higher stagnation pressures and temperatures than reflected shock tunnels and therefore they enlarge the simulation range, especially the pL-U scaling capability. However, limitations are given by limited driver performances and, in particular, by the short testing time which significantly limits the maximum tolerable model size. Hence, increasing the test section size of expansion tunnels by increasing the nozzle area ratio is rather pointless. The only way to test larger models in an expansion tunnel is by scaling the entire facility. This therefore results in huge costs because the expansion tunnel would have to be at least about twice as long and have approximately at least twice the inner tube diameter compared to the smallest reflected shock tunnel which can test the given model size. Nonetheless, depending on the application, expansion tunnels might sometimes be selected over reflected shock tunnels even for low and medium enthalpy conditions because expansion tunnels produce test flows with less thermochemical excitation. This is the result of the total enthalpy and total pressure multiplication feature of the unsteady expansion and the fact that the test gas is only shock processed once in the expansion tunnel. For example, the LENS XX facility allows the testing of models of feasible size at moderate total enthalpies resulting in sufficiently long testing times. In this way the advantage of less thermochemical excitation of the freestream can be utilized for high quality testing. So, experimental research in modern hypersonics involves the use of a variety of different test facilities, each with its own unique capabilities and limitations.

Declaration of competing interest

The authors declare the following financial interests/personal relationships which may be considered as potential competing interests: Most of the material has been presented as lecture notes titled "Operation, capabilities and limitations of existing hypersonic facilities" in The von Karman Institute for Fluid Dynamics (VKI) Lecture Series AVT-325 (Flow characterization and modelling of hypersonic wind tunnels) in 2018.

Acknowledgements

The author would like to acknowledge Steven Lewis and Chris James of the Centre for Hypersonics at The University of Queensland for providing the performance envelop of the X2 expansion tunnel, Sam Stennett and Andreas Andrianatos of the Centre for Hypersonics at The University of Queensland for providing information on the X3 facility, Chen Xing of the China Academy of Aerospace Aerodynamics for providing information on the FD-21 facility and Qiu Wang from the Chinese Academy of Sciences for information about JF12.

- Hypersonic Test Facil. (2002) 29–71, <https://doi.org/10.2514/5.9781600866678.0029.0071>.
- [118] A. Paull, R. Stalker, I. Stringer, Experiments on an expansion tube with a free piston driver, 15th Aerodyn. Test. Conf. (1988), <https://doi.org/10.2514/6.1988-2018>.
- [119] D.R. Bartz, A simple equation for rapid estimation of rocket nozzle convective heat transfer coefficients, *Jet Propul.* 27 (1957) 49–51.
- [120] H. Tanno, T. Komuro, K. Sato, K. Itoh, M. Takahashi, K. Fujita, S. Laurence, K. Hannemann, Free-flight force measurement technique in shock tunnel, 50th AIAA Aerosp. Sci. Meet. Incl. New Horizons Forum Aero. Expo. (2012), <https://doi.org/10.2514/6.2012-1241>.